Elsevier Editorial System(tm) for Materials Characterization

Manuscript Draft

Manuscript Number: MTL-15097R1

Title: IDENTIFICATION OF THE MECHANISM THAT CONFERS SUPERHYDROPHOBICITY ON 316L STAINLESS STEEL

Article Type: Research paper

Keywords: Superhydrophobicity; stainless steel; coating; electrolytic reaction; self assembly; hierarchical structures

Corresponding Author: Mrs. ANA M. ESCOBAR,

Corresponding Author's Institution: UNIVERSITAT DE BARCELONA

First Author: ANA M. ESCOBAR

Order of Authors: ANA M. ESCOBAR; NÚRIA LLORCA-ISERN; ORIOL RIUS-AYRA

Abstract: This study develops a rapid method to confer superhydrophobicity on 316L stainless steel surfaces with an amphiphilic reagent such as dodecanoic acid. The highest contact angle (approaching 173°) was obtained after forming hierarchical structures with a non-aqueous electrolyte by an electrolytic process. Our goal was to induce superhydrophobicity directly on 316 stainless steel substrates and to establish which molecules cause the effect. The superhydrophobic behaviour is analysed by contact angle measurements, scanning electron microscopy (SEM), IR spectroscopy and atomic force microscopy (AFM). The growth mechanism is analysed using FE-SEM, TOF-SIMS and XPS in order to determine the molecules involved in the reaction and the growth. The TOF-SIMS analysis revealed that the Ni2+ ions react with lauric acid to create an ester on the stainless steel surface.

Suggested Reviewers: Dilip Sarkar
UNIVERSITY RESEARCH CENTER ON ALUMINUM, University of Quebec
dsarkar@uqac.ca

DANICK GALLANT
ALUMINUM TECHNOLOGY CENTRE, NATIONAL RESEARCH COUNCIL OF CANADA

NASER VALIPOUR
Department of Chemistry, University of Birjand

Edward Bormashenko
Department of Physics, Ariel University

**Cover letter**

The aim of the study was to obtain superhydrophobic 316L stainless steel using a direct method and identifying the mechanism involved. Until now, fabrication techniques of hydrophobic stainless steel surfaces have been limited because they require special equipment, complex process and long period process as sol-gel process, chemical vapour deposition, laser treating or anodic oxidation. In the present study, superhydrophobicity is obtained by chemical reaction between nickel ions and lauric acid on stainless steel surface. Additionally, we have performed a complete characterization of this material by different techniques in order to identify the molecules responsible for superhydrophobicity, the mechanism by which superhydrophobicity is produced, and consequently the influence of variables such as reaction time in the proposed processing method.

We consider that our manuscript fulfils several aspects to which Materials Characterization is focussed, such as the elucidation of the mechanism involved in the particular surface modification of the stainless steel as well as the characterization of the reaction products at the nanoscale.

Ana Maria Escobar

Núria Llorca-Isern

Oriol Rius-Ayra

**Authors**

*Ana Maria Escobar*, corresponding autor. CPCM Departament de Ciència dels Materials i Enginyeria Metal·lurgica, Facultat de Química, Universitat de Barcelona, Marti-Franqués 1, 08028 Barcelona, Spain, +34934021111, annaescobarromero@ub.edu.

*Núria Llorca-Isern*, CPCM Departament de Ciència dels Materials i Enginyeria Metal·lurgica, Facultat de Química, Universitat de Barcelona, Marti-Franqués 1, 08028 Barcelona, Spain, +34934021111, nullorca@ub.edu.

*Oriol Rius-Ayra,* CPCM Departament de Ciència dels Materials i Enginyeria Metal·lurgica, Facultat de Química, Universitat de Barcelona, Marti-Franqués 1, 08028 Barcelona, Spain, +34934021111, jriusayr8@alumnes.ub.edu

## *Reviewers' comments:*

The authors would like to thank the reviewers for making very valuable comments that have improved our research.

*Reviewer #1: The submitted manuscript presented a new method for superhydrophobic surface preparation by direct electrolysis of a non-aqueous solution containing nickel salt and lauric acid. Though the growth kinetics was intensively investigated, the detailed mechanism concerning which reagents are the key parameters for superhydrophobicity generation is still unclear.*

In the revised version we include a more detailed explanation of the involved reagents.

... Based on our XPS and TOF-SIMS analysis and the obtained results, the proposed reaction mechanism for the as-prepared superhydrophobic coatings involves the $Ni^{2+}$ ions around the cathode plate being reduced to metallic nickel on the cathodic surface when the voltage is applied across the two 316L stainless steel electrodes. The metallic nickel will then act as growth site resulting an essential actor in the mechanism. Meanwhile, more $Ni^{2+}$ ions near the cathodic plate will react with the lauric acid and form nickel laureate on the activated surface of the 316L stainless steel using metallic nickel as anchorage agent or growth site. The reaction processes can be formulated as follows:

**Scheme 1.** Redox reaction

$Fe_{(s)} \rightarrow Fe_{(aq)}^{2+} + 2\,\bar{e}$

$Ni_{(aq)}^{2+} + 2\bar{e} \rightarrow Ni_{(s)}$ (growth site)

**Scheme 2.** Laureate formation

$Ni_{(aq)}^{2+} + CH_3(CH_2)_{10}COOH_{(aq)} \rightarrow Ni[CH_3(CH_2)_{10}COO]_2 + 2H_{(aq)}^{+}$

Previous studies using cobalt also showed superhydrophobic results[36] due to the similar reduction potential character of this metal confirning that the reduction step of the metal ions present in the electrolyte solution as growth sites and anchorage agent is critical for the self-organisation process.

*The manuscript should be improved by providing some neccessary control experiments when describing the role of Ni ion. I suggest the authors give additional experimental data including the coatings prepared from electrolytes containing dodecanoic acid-alone, and those contianing other metallic ions (such as copper) to clearly confirm which reagents are the key parameters for the formation of superhydrophobicity.*

-We have included the results of three additional set of samples using different electrolyte solutions in order to describe and suggest the role of the reagents.

We include at the manuscript the following paragraph:

...Three sets of samples, named A, B and C, respectively, were prepared changing just the electrolyte composition in order to evaluate the importance of each reagent in the reaction taking place in the process. Samples A were prepared into an electrolyte solution of ethanol, samples B were prepared into an electrolyte solution of nickel chloride (0.05 M) in ethanol and finally, samples C were prepared into an

electrolyte solution of lauric acid (0.1 M) in ethanol. The etching time was 900 seconds for all the samples....

...All the three sets of samples A, B and C, showed completely hydrophilic behaviour. These results confirm that lauric acid, metallic nickel and nickel ion are altogether essential actors in the reaction....

-Chen et al (2013, reference 36) produced superhydrophobic surfaces via electrodeposition with cobalt salts. One main reason for the satisfactory results obtained with our method using nickel salts is because nickel and cobalt had similar electrolytic potential. As copper electrolytic potential is quite different from that of nickel and cobalt when using copper salt as reagent instead of nickel salt did not produce superhydrophobic surfaces.

*In addition, some basic information, like film thickness and roughness, and mechanical property (e.g. adhesion, anti-abrasive property, etc.)should be given.*

-Film thickness has been analized by FE-SEM. Cross sections of the samples were observed and the results were incorporated in the manuscript.

... FESEM micrographs of cross section had allowed to measure the film thickness, sample 1 shows the highest value with 3.5±0.6 micrometers and the lowest value of superhydrophobic samples is 2.2 ±0.5 corresponding to sample 7....

-The authors, considering that the knowledge of the mechanism involved in the hydrophobic character achieved for stainless steel, want to emphasise that this research is focussed on this mechanism and they believe that this is critical in order to enhance and stabilise this significant property in particular for AISI 316L. The properties and behaviour other than hydrophobicity will be studied in the near future.

*Title Page

# IDENTIFICATION OF THE MECHANISM THAT CONFERS SUPERHYDROPHOBICITY ON 316L STAINLESS STEEL

*Ana M. Escobar*[*1], Nuria Llorca-Isern[1], Oriol Rius-Ayra[1]*

*corresponding author

[1] CPCM Departament de Ciència dels Materials i Enginyeria Metal·lurgica, Facultat de Química, Universitat de Barcelona, Marti-Franqués 1, 08028 Barcelona, Spain

*Information Authors:*

*Ana Maria Escobar*, corresponding autor. CPCM Departament de Ciència dels Materials i Enginyeria Metal·lurgica, Facultat de Química, Universitat de Barcelona, Marti-Franqués 1, 08028 Barcelona, Spain, +34934021111, annaescobarromero@ub.edu.

*Núria Llorca-Isern*, CPCM Departament de Ciència dels Materials i Enginyeria Metal·lurgica, Facultat de Química, Universitat de Barcelona, Marti-Franqués 1, 08028 Barcelona, Spain, +34934021111, nullorca@ub.edu.

*Oriol Rius-Ayra,* CPCM Departament de Ciència dels Materials i Enginyeria Metal·lurgica, Facultat de Química, Universitat de Barcelona, Marti-Franqués 1, 08028 Barcelona, Spain, +34934021111, jriusayr8@alumnes.ub.edu

ABSTRACT This study develops a rapid method to confer superhydrophobicity on 316L stainless steel surfaces with an amphiphilic reagent such as dodecanoic acid. The highest contact angle (approaching 173°) was obtained after forming hierarchical structures with a non-aqueous electrolyte by an electrolytic process. Our goal was to induce superhydrophobicity directly on 316 stainless steel substrates and to establish which molecules cause the effect. The superhydrophobic behaviour is analysed by contact angle measurements, scanning electron microscopy (SEM), IR spectroscopy and atomic force microscopy (AFM). The growth mechanism is analysed using FE-SEM, TOF-SIMS and XPS in order to determine the molecules involved in the reaction and the growth. The TOF-SIMS analysis revealed that the $Ni^{2+}$ ions react with lauric acid to create an ester on the stainless steel surface.

**Graphical Abstract (for review)**

# HIGHLIGHTS

This study develops a rapid and facile approach to impart superhydrophobicity properties to 316L stainless steel surfaces with an amphiphilic reagent such as dodecanoic acid. This process changes the surface character from superhydrophilicity to superhydrophobicity.

The process based on electrolysis of a nickel salt in lauric acid provides superhydrophobic behaviour in 316L stainless steel.

The growth mechanism is proposed as a mode island (Volmert- Weber mode).

TOF-SIMS and XPS provided the identification of the molecules involved in the surface modification reaction on AISI 316L inducing superhydrophobicity .

*Text Only in MS Word (Double-Spaced)
Click here to view linked References

# IDENTIFICATION OF THE MECHANISM THAT CONFERS SUPERHYDROPHOBICITY ON 316L STAINLESS STEEL

*Ana M. Escobar*[1], Nuria Llorca-Isern[1], Oriol Rius-Ayra[1]*

*corresponding author

[1] CPCM Departament de Ciència dels Materials i Enginyeria Metal·lurgica, Facultat de Química, Universitat de Barcelona, Marti-Franqués 1, 08028 Barcelona, Spain

ABSTRACT This study develops a rapid method to confer superhydrophobicity on 316L stainless steel surfaces with an amphiphilic reagent such as dodecanoic acid. The highest contact angle (approaching 173°) was obtained after forming hierarchical structures with a non-aqueous electrolyte by an electrolytic process. Our goal was to induce superhydrophobicity directly on 316 stainless steel substrates and to establish which molecules cause the effect. The superhydrophobic behaviour is analysed by contact angle measurements, scanning electron microscopy (SEM), IR spectroscopy and atomic force microscopy (AFM). The growth mechanism is analysed using FE-SEM, TOF-SIMS and XPS in order to determine the molecules involved in the reaction and the growth. The TOF-SIMS analysis revealed that the $Ni^{2+}$ ions react with lauric acid to create an ester on the stainless steel surface.

KEYWORDS Superhydrophobicity; stainless steel; coating; electrolytic reaction; self assembly; hierarchical structures.

## 1. INTRODUCTION

Superhydrophobic surfaces, with extremely high water contact angles (CAs) of more than 150° are of special interest due to their various anti-adhesive and self-cleaning properties [1]. A closely related phenomenon in nature is the lotus effect, which refer to surfaces that are difficult to wet. Recent studies demonstrate that the superhydrophobicity of lotus leaves principally results from the presence of binary structures at both the micrometer and nanometer scales together with the low-energy wax-like materials on the surfaces [2]. Materials with similar properties, to those of the lotus leaf structure are very useful in several areas, such as the aeronautical industry [3, 4] and civil engineering [5], so many methods have been developed to mimic the lotus leaf structure. Metals are very important and irreplaceable engineered materials in many industrial fields. Stainless steel is one of the most common metals or alloys; it is widely used in industry due its good mechanical workability and anticorrosion properties. Nevertheless, fabrication of superhydrophobic stainless steel has remained relatively unstudied compared to other metals such as zinc, copper or aluminium [6-10].

The wettability of solid substrates is known to be dependent on both their chemical composition and their topographic structure, either lowering the surface energy with different molecules [11, 12] or increasing surface roughness (through techniques such as sand-blasting [13] chemical etching [14] or grinding processes), reduces the affinity of water drops to the surface. Combining the appropriate surface roughness and low surface energy material leads to artificial superhydrophobic surfaces inspired by the lotus leaf [15], rose petal [16], leg of the water strider [17] and other natural surfaces with self-cleaning and water-repellent properties [18]. Until now, techniques to fabricate superhydrophobic stainless steel surfaces have been limited because they require special equipment, complex

processes or a considerable period of time; this is the case with the sol-gel process, chemical vapour deposition, laser treating and anodic oxidation [19-25]. Consequently, there is a need to develop a simple and rapid method for conferring superhydrophobicity on stainless steel surfaces, as could be envisaged through electrolytic coating at room temperature [26]. Here, in order to reduce the reaction time and simplify the procedure, we propose a two-step process: the initial step is to grind the 316L stainless steel surface to increase surface roughness, and the second, to reduce the surface energy of the substrate by electrodeposition of a metal-fatty acid. Superhydrophobicity is produced by the chemical reaction between nickel ions and lauric acid on a 316L stainless steel surface. The present study has three main objectives: to identify the molecules responsible for superhydrophobicity, the mechanism by which superhydrophobicity is produced, and consequently the influence of variables such as reaction time on the proposed processing method. We use time-of-flight secondary ion mass spectrometry (TOF-SIMS) and X-ray photoelectron spectroscopy (XPS) techniques to identify the molecules involved in the growth step, by paying close attention to the analysis of the mechanism by which the chemical reaction proceeds.

## 2. EXPERIMENTAL PROCEDURE

Pieces of commercial 316L stainless steel, 15 x 50 x 2 mm, were used as the substrate for this study. All the samples were produced by the same process, the details of which are as follows. First, the cleaned samples were ground with SiC abrasive paper ranging from an average particle diameter of 63 μm (P220 grade) to 15.3 μm “super fine” (P1200 grade). Second, the samples were ultrasonically cleaned with ethanol followed by deionized water and then, they were dried with forced air. Third, two cleaned samples were immersed

vertically into a uniform electrolyte solution of nickel chloride (0.05 M) and lauric acid (0.1 M) in ethanol, 3 cm apart: they were used as the cathode and the anode of an electrolyte cell, and a direct current (DC) voltage of 30 V was applied across the two electrodes. The etching time were modified from 900 to 10 seconds in order to evaluate the growth mechanism of the coating, until hydrophilic surfaces were obtained. After the selected electrolysis time, the working electrodes were immediately rinsed with ethanol and deionized water and dried in air, giving the as-prepared cathodic surface. Consecutive numbers were assigned to the samples in order to identify each electrolysis condition with its corresponding sample; the surface produced after 900 seconds of electrolysis was numbered 1 and the rest of the specimens were numbered following the descending order of electrolysis times as shown in Table 1.

Table 1. Electrolysis time for the different set of samples.

| **Sample** | **1** | **2** | **3** | **4** | **5** | **6** | **7** | **8** |
|---|---|---|---|---|---|---|---|---|
| **Electrolysis time/ s** | 900 | 600 | 300 | 60 | 30 | 20 | 15 | 10 |

Three sets of samples, named A, B and C, respectively, were prepared changing just the electrolyte composition in order to identify the importance of each reagent in the reaction taking place in the process. Samples A were prepared into an electrolyte solution of ethanol, samples B were prepared into an electrolyte solution of nickel chloride (0.05 M) in ethanol and finally, samples C were prepared into an electrolyte solution of lauric acid (0.1 M) in ethanol. The etching time was 900 seconds for all the samples.

The specimen surface was characterized using a Hitachi S-4100 field emission scanning electron microscope (FE-SEM) in order to study their morphological features. Atomic force microscopy (AFM) measurements were taken using a Dimension 3100 microscope attached to Nanoscope IV electronics (Bruker) using Si probes with a nominal spring constant of 40 nN/nm (T300R-W, Vistaprobes). All the topographic measurements were performed in tapping mode at a scan rate of 0.3Hz and 512x512 pixels resolution. The samples were imaged in air and at 55% RH. The AFM measurements were carried out in Peak Force Scan Asyst mode (QNM) in order to quantify the Young's modulus of the surfaces. The initial roughness was measured by confocal microscopy using LeicaScan DCM 3D on a surface of 1.21x 0.91 mm. The reported roughness values are the average of three measurements at different places on the surface. The chemical groups of the superhydrophobic coatings were determined by infrared absorption spectroscopy (Thermo Scientific Nicolet IN10MX). The chemical composition of the surface was analysed by X-ray photoelectron spectroscopy in a PHI 5500 Multitechnique System (Physical Electronics) with a monochromatic X-ray source (Aluminium Kα line of 1486.6 eV and 350 W) on 0.8 mm diameter discs. All measurements were made in an ultra-high vacuum (UHV) chamber pressure between $5x10^{-9}$ and $2x10^{-8}$ torr. The carbon 1s line was used to calibrate the binding-energy scale for XPS measurements, for which a binding energy of 284.8 eV was assumed. High-resolution mass spectra of positive and negative secondary ions were obtained using TOF-SIMS IV (ION-TOF, Munster, Germany) equipment operating at a pressure of $5 \times 10^{-9}$ mbar with a 25 keV pulsed bismuth liquid metal ion source ($Bi_3^{++}$). Secondary ions were detected with a reflector TOF analyser, multichannel plates (MCPs), and a time-to-digital converter (TDC). Measurements were performed with a typical acquisition time of 10 s, at a TDC time resolution of 200 ps and a 100 µs cycle time. Secondary ion spectra were acquired from

randomly rastered sample surface areas of 100 x 100 μm. Mass spectral acquisition was performed using the ION-TOF Ion Spec software (version 4.1). Finally, CA were measured with a Contact Angle Measuring System DSA 100 from KRÜSS with 10 μL of deionized water at room temperature. The reported CA values are the average of three measurements of CA of droplets at different places on the surface. Sliding angles were measured by dropping a water droplet on a superhydrophobic sample positioned on a tilting stage. The tilting angle of the stage was adjusted using a micrometer with a resolution of 0.5°. Sliding angles values are the average of three measurements of droplets at different places on the surface, the standard deviation were calculated and it is minor than 1° in all the measured samples.

## 3. RESULTS AND DISCUSSION

Samples were prepared using the procedure outlined above. In order to produce superhydrophobic surfaces on 316L stainless steel, we reduced the electrolysis time from 900 seconds down to the minimum necessary to produce a hydrophilic surface, using the same materials and coating method. An electrolysis time of 10 seconds was enough to generate hydrophilic stainless steel. The growth mechanism of the coating was thus studied.

Surface wettability was evaluated by static CA measurements of hydrophobic samples and the 316L stainless steel substrate. As shown in Figure 1, there is no obvious correlation between electrolysis time and hydrophobic effect in this experiment. The highest CA was 175° at 30 seconds (sample 5) with a sliding angle of 3.5° and the lowest CA was 160° at both 20 s (sample 6) and 600 seconds (sample 2) with sliding angles of 5° and 4.5°, respectively. The 316L stainless steel substrate had hydrophilic properties with a CA of 40°. In summary, the procedure to make a superhydrophobic surface does not need much

time: 30 seconds of electrolysis time was sufficient to achieve maximum superhydrophobicity.

Figure 2 shows the typical morphology of the surface after 30 seconds of electrolysis (sample 5); top right, top left and bottom left are the SEM micrographs with low and high magnification, respectively. It can clearly be seen that the surface of 316L stainless steel is textured with 2 μm pillars along the grinding direction. In greater detail, we can also observe that the surfaces of the pillars are covered by nanoscale granular protrusions. These hierarchical micro-nano structures have grooves that trap a fraction of the air, thereby favouring the hydrophobicity of the material. The EDS spectrum (Fig. 2d), suggests that the composition of the coating is mostly Ni and O.

Figure 3 (a-h) shows the surface morphology of the samples 1 to 8 after different electrolysis times. The microstructure of all the surfaces is formed mainly of pillars and islands. Surfaces 1, 2 and 3 (900, 600 and 300 seconds of electrolysis, respectively) are completely coated and mainly formed of islands; whereas surfaces with shorter electrolysis times (samples 4, 5, 6 and 7) are only partially covered, showing that the coating initially generates pillars, which suggests a process related to the Volmert-Weber growth mode, as can be observed in some areas of the substrate. The surface of sample 8 has widely dispersed pillars (Fig. 3h), this sample is not superhydrophobic. Bubble-like protuberances with different diameters between 2 and 5 μm are observed on all the samples.

From the mechanism point of view, the building block is the pillar, followed by the island formation which is a connected group of pillars. It is not necessary that both cover the entire surface for producing superhydrophobicity.

FESEM micrographs of cross section had allowed to measure the film thickness, sample 1 shows the highest value with 3.5±0.6 micrometers and the lowest value of superhydrophobic samples is 2.2 ±0.5 corresponding to sample 7.

AFM images (1 x 1 $\mu m^2$ area) were produced to compare the final roughness of the superhydrophobic specimens using RMS roughness as a comparison parameter; and also to calculate their Young's modulus. Both results are summarized in Table 2.

Table 2. RMS and E from AFM analysis of coated samples.

| **Sample** | **Prepared substrate** | **1** | **2** | **3** | **4** | **5** | **6** | **7** |
|---|---|---|---|---|---|---|---|---|
| **RMS/nm** | 210 | 55 | 20 | 12 | 45 | 39 | 124 | 189 |
| **E/GPa** | 200 | 0.20 | 0.5 | 0.25 | 0.58 | 0.41 | 0.29 | 0.04 |

The AFM images are shown in Figure 4. The surface roughness resulting from the AFM analysis of the coated samples indicates that the highest RMS value corresponds to the sample that underwent the least electrolysis time. This can be explained by the treatment only generating pillars without connections between them. In contrast, samples that underwent longer electrolysis times have neighbouring pillars connected, forming a more homogeneous surface with less roughness. These results are consistent with our FE-SEM analysis. The Young's modulus values are very low due to the organic nature of the coating, compared to the substrate AISI 316L modulus (200 GPa).

AFM analysis allowed us to measure the width of the pillars in the initial step of the growth mechanism on the samples that underwent the shortest electrolysis time. Figure 5 shows the surface of sample 6 with vertical distance values between 104 and 146 nm; whereas the

surface of sample 7 has vertical distance of 70 to 212 nm. In accordance with these results, it can be concluded that 70-100 nm is the minimum height of pillars necessary to obtain superhydrophobic 316L stainless steel using a lauric acid-nickel chloride-ethanol medium.

The SEM and AFM analysis confirmed that the coating starts with the formation of pillars, then, the islands morphology results when several pillars grow together. Finally the surface of the sample is completely covered (as shown after 300 seconds of electrolysis).

In order to confirm the chemical composition of the as-prepared coatings, IR, TOF-SIMS and XPS techniques were used. Figure 6 shows IR spectra of the as-prepared coatings (the samples with the shortest electrolysis times (samples 6 and 7) were not observed by this technique). The IR spectra indicate that the free acidic group band from the lauric acid at 1702 $cm^{-1}$ is no longer present, compared to the MICC-73396-421X spectrum (CAS registry number 143-07-7, CAS index name dodecanoic acid) [27], whereas the peak at 1590 $cm^{-1}$ corresponding to coordinated ester groups appears as in the NIDA71076 spectrum (CAS registry number 13282-11-6, CAS index name dodecanoic acid, $nickel^{2+}$ salt (2:1)) [28]. Therefore, it can be concluded that $(CH_3(CH_2)_{10}COOH$ changed into $(CH_3(CH_2)_{10}COO^-$. The two peaks at 2850 and 2922 $cm^{-1}$ belong to the symmetric and asymmetric C-H stretching modes of the $CH_2$ groups of laureate, respectively. This supports the previous finding.

TOF-SIMS was used to study the chemical reactions and lateral distributions of fatty acids enhanced to react on 316L stainless steel surfaces. On these alloy surfaces, a direct interaction between the acid and nickel ions is observed via detection of a molecular ion that corresponds to the mass of the laureate anion, nickel cation and $Ni[laureate]_2$. Since TOF-SIMS can detect and discriminate specific chemical reaction products, it was used to

identify reaction products formed between the fatty acid molecules, nickel ions and metallic surface. The positive secondary ion mass spectra for sample 6 (20 s of electrolysis is shown at Fig. 7. The assignments are based upon classical mass spectroscopic fragmentation patterns [29]. Wandass et all, [30] studied different fatty acids on silver surfaces using TOF-SIMS, including lauric acid and they obtained similar signals to those obtained in our study. The peaks represent masses of: 100 units, which corresponds to $(CH_2CONi)^+$; 133 units, for $(CH_3CH_2COONi)$; 266 units, for $Na(CH_3(CH_2)_9COONi)^+$, (Na is considered a contaminant that is easily detected by SIMS); and 411 units, for $(CH_3(CH_2)_{10}COO\text{-}Ni\text{-}OOC(CH_2)_{10}CH_3 + H\text{-}HCOOH)^+$. The presence of these species on the stainless steel surface was also confirmed by the XPS Ni 2p and O 2s signals.

XPS was used to characterize the coating on the 316L stainless steel and to determine its composition. We analysed all seven samples from 15 to 900 s of electrolysis, considering oxygen, carbon and nickel peaks. In all the samples, the peaks were repeated at the same value of the binding energy. Figure 8 shows the superhydrophobic sample spectra. The peak at 852 eV is attributed to Ni metal; its intensity decreases as the process time increases because after less than 30 seconds of electrolysis the coating is thicker after more than 60 seconds of electrolysis. After less than 30 seconds, XPS detected Ni metal from the substrate and also Ni metal in the coating; in contrast to the results after more than 60 seconds of electrolysis, when XPS mostly detected Ni metal formed by the reaction.

Figure 9 shows two examples of C (top) and O (bottom) deconvolution corresponding to sample 5 and sample 1. The peak located at 284.6 eV is attributed to C-1s and its deconvolution gives three peaks: the first is located at 288 eV and it is attributed to the

carbonyl of lauric acid [31, 32]; the second is at 286 eV corresponding to the ester group [32]; while the third is at 284 eV and it is attributed to adventitious carbon [32] (Fig. 9top). The peak located at 531.7 eV is attributed to O-2s and its deconvolution also gives three peaks; the binding energy of the first is 529 eV and it is attributed to NiO; the second is located at 531 eV and it is attributed to $Ni(OH)_2$; and the last located at 532 eV is attributed to the C-O bond [33] (Fig 9bottom). The peak located at 856.5 eV is attributed to Ni-$2p_{3/2.}$ Its deconvolution again gives three new peaks; the first located at 852 eV is attributed to Ni metal; the second at 856 eV is attributed to $Ni(OH)_2$; and the last at 861 eV is attributed to a satellite of the previous compound and so it also corresponds to $Ni(OH)_2$ [34]. Finally, the peak located at 711 eV corresponds to the Fe-$2p_{3/2}$ from the stainless steel substrate. [35]

The XPS results reveal the presence of metallic nickel and also oxidized nickel corresponding to the $Ni[CH_3(CH_2)_{10}COO)]_2$ molecule. A similar product was also observed by Chen et al [36] in their research on cobalt-based coatings using X ray diffraction techniques. In the present study, the TOF-SIMS results confirm the bonding between lauric acid and Ni, as well as the existence of metallic nickel.

One factor that promotes superhydrophobicity can be attributed to the chemical composition of the surface on which superhydrophobicity will appear. A chemical reaction will be associated with each part of the process that produces the change to superhydrophobicity of the 316L stainless steel surface.

Samples A, B and C, have completely hydrophilic behaviour, these results confirms that lauric acid, metallic nickel and nickel ion are together essential reagents.

Based on our XPS and TOF-SIMS analysis and the obtained results, the proposed reaction mechanism for the as-prepared superhydrophobic coatings involves the $Ni^{2+}$ ions around the cathode plate being reduced to metallic nickel on the cathodic surface when the

voltage is applied across the two 316L stainless steel electrodes. The metallic nickel will then act as growth site resulting an essential actor in the mechanism.. Meanwhile, more $Ni^{2+}$ ions near the cathodic plate will react with the lauric acid and form nickel laureate on the activated surface of the 316L stainless steel using metallic nickel as anchorage agent or growth site. The reaction processes can be formulated as follows:

**Scheme 1.** Redox reaction

$$Fe_{(s)} \rightarrow Fe_{(aq)}^{2+} + 2\,\bar{e}$$

$$Ni_{(aq)}^{2+} + 2\bar{e} \rightarrow Ni_{(s)}\,(\text{growth site})$$

**Scheme 2.** Laureate formation

$$Ni_{(aq)}^{2+} + CH_3(CH_2)_{10}COOH_{(aq)} \rightarrow Ni[CH_3(CH_2)_{10}COO]_2 + 2H_{(aq)}^{+}$$

Previous studies using cobalt also showed superhydrophobic results[36] due to the similar reduction potential character of this metal confirning that the reduction step of the metal ions present in the electrolyte solution as growth sites and anchorage agent is critical for the self-organisation process.

## 4. CONCLUSIONS

Superhydrophobic surfaces on 316L stainless steel were developed via a short procedure consisting of the electrolysis of stainless steel in the lauric/nickelchloride/ethanol electrolyte. 30 seconds of reaction was enough to obtain an optimum superhydrophobic 316L stainless steel surface (CA 175°).

Reducing the electrolysis time allowed us to identify the growth mechanism as three-dimensional islands (Volmert-Weber mode) thus leading to the superhydrophobicity via

simultaneous pillar growth. Consequently, from the mechanism point of view, the building block is the pillar, followed by the island formation which is a connected group of pillars. Experimentally it is found that it is not necessary that both cover the entire surface for producing superhydrophobic character.

From the property point of view, the characteristic magnitude seems to be the vertical height of the pillars and the islands for producing superhydrophobicity. We used AFM to stablish the minimum range of vertical height of the pillars necessary to obtain superhydrophobic 316L stainless steel.

TOF-SIMS and XPS analysis allowed us to identify the species responsible for the superhydrophobicity on the 316L stainless steel substrate as $CH_3(CH_2)_{10}COONiOH$ and $(CH_3(CH_2)_{10}COO)_2Ni$.

Superhydrophobicity is associated to the redox reaction of $Fe/Ni^{2+}$ to $Fe^{2+}/Ni$, with Ni as the growth site, and also with the laureate formation reaction.

## 5. REFERENCES

[1] B. Bhushan, Y.C. Jung, Natural and biomimetic artificial surfaces for superhydrophobicity, self-cleaning, low adhesion, and drag reduction, Prog. Mater. Sci. 56 (2011) 1-108.

[2] N. Valipour, F. Ch. Birjandi, J. Sargolzaei, Super-non-wettable surfaces: A review, Colloids and Surfaces A: Physicochem. Eng. Aspects 448 (2014) 93-106.

[3] J. Ou,W. Hu, M. Xue, F. Wang, W. Li, Superhydrophobic surfaces on light alloy substrates fabricated by a versatile process and their corrosion protection, ACS Appl. Mater. Interfaces 5 (2013) 3101-3107.

[4] J. Xiao, S. Chaudhuri, Design of anti-icing coatings using supercooled droplets as nano-to-microscale probes, Langmuir 28 (2012) 4434-4446.

[5] Y. Huang, D.K. Sarkar, D. Gallant, X-Grant Chen, Corrosion resistance properties of superhydrophobic copper surfaces fabricated by one-step electrochemical modification process, App. Surf. Sci. 282 (2013) 689-694.

[6] Y. Wan, Z. Wang, Z. Xu, C. Liu, J. Zhang, Fabrication and wear protection performance of superhydrophobic surface on zinc, App. Surf. Sci. 257 (2011), 7486-7489.

[7] P. Li, X. Chen, G. Yang, L. Yu, P. Zhang, Preparation of silver-cuprous oxide/stearic acid composite coating with superhydrophobicity on copper substrate and evaluation of its friction-reducing and anticorrosion abilities, App. Surf. Sci. 289 (2014) 21-26.

[8] A. M. Escobar, N. Llorca-Isern, Superhydrophobic coating deposited directly on aluminium, App. Surf. Sci. 305 (2014) 774-782.

[9] J. Ou, W. Hu, M. Xue, F. Wang, W. Li, One-step solution immersion process to fabricate superhydrophobic surfaces on light alloys, ACS Appl. Mater. Interfaces 5 (2013) 9867-9871.

[10] X. Zhu, Z. Zhang, X. Men, J. Yang, K. Wang, X. Xu, X. Zhou, Robust superhydrophobic surfaces with mechanical durability and easy repairability, J. Mater. Chem (2011), DOI:10.1039/c1jm12513.

[11] A. Nouri, C. Wen, Surfactants in mechanical alloying/milling: a catch-22 situation, Critical Reviews in solid state and materials Sciences 39 (2014) 81-108.

[12] L. Boinovich, A. Emelyanenko, V. Ivanov, A. Pashinin, Durable icephobic coating for stainless steel, ACS Appl. Mater. Interfaces 5 (2013) 2549-2554.

[13] M. Frank, A. Boccaccini, S. Virtanen, A facile and scalable method to produce superhydrophobic stainless steel surface, Appl. Surf. Sci. 311 (2014) 753-757.

[14] L. Li, V. Breedveld, D. Hess, Creation of superhydrophobic stainless steel surfaces by acid treatments and hydrophobic film deposition, ACS Appl. Mater. Interfaces 4 (2012) 4549-4556.

[15] L. Chen, Z. Xiao, P. Chan, Y. Lee, Static and dynamic characterization of robust superhydrophobic surfaces built from nano-flowers on silicon micro-post arrays, J. Micromech. Microeng. 20 (2010) 105001.

[16] Y. Liu, J. Liu, S. Li, Z. Han, Fabrication of biomimetic super-hydrophobic surface on aluminum alloy, J. Mater Sci. 49 (2014) 1624-1629.

[17] D. Hu, B. Chan, J. Bush, The hydrodynamics of water strider locomotion, Nature 424 (2003) 663-666.

[18] Y. Zhang, Q. Chen, E. Kim, H. Sun, Biomimetic grapheme films and their properties, Nanoscale 4 (2012) 4858-4869.

[19] Y. Yan, N. Gao, W. Barthlott, Mimicking natural superhydrophobic surfaces and grasping the wetting process: a review on recent progress in preparing superhydrophobic surfaces, Advanced in Colloid and Interface Science 169 (2011) 80-105.

[20] M. Kavale, S. Mahadik, D. Mahadik, V. Parale, A. Rao, R. Vhatkar, P. Wagh, S. Gupta, Enrichment in hydrophobicity and scratch resistant properties of silica films on glass by grafted microporosity of the network, J. Sol-Gel Sci. Technol. 64 (2012) 9-16.

[21] K. Ellinas, S. Pujari, D. Dragatogiannis, C. Chariditis, A. Tserepi, H. Zuilhof, E. Gogolides, Plasma micro-nanotextured, scratch, water and hexadecane resistant, superhydrophobic and superamphiphobic polymeric surfaces with prefluorinated monolayers, ACS Appl. Mater. Interfaces 6 (2014) 6510-6524.

[22] A. Leon, R. Pernites, R. Advincula, Superhydrophobic colloidally textured polythiophene film as superior anticorrosion coating, ACS Appl. Mater. Interfaces 4 (2012) 3169-3176.

[23] F.J. Wang, S. Lei, J.F. Ou, M.S. Xue, W. Li, Superhydrophobic surfaces with excellent mechanical durability and easy repairability, Appl. Surf. Sci. 276 (2013) 397-400.

[24] C. Badre, P. Dubot, D. Lincot, T. Pauporte, M. Turmine, Effects of nanorod structure and conformation of fatty acid self-assembled layers on superhydrophobicity of zinc oxide surface, J. Colloid Interface Sci. 316 (2007) 233-237.

[25] D. Ebert, B. Bhushan, Durable lotus-effect surfaces with hierarchical structure using micro- and nanosized hydrophobic silica particles, J. Colloid Interface Sci. 368 (2012) 584-591.

[26] T. Darmanin, F. Guittard, Homogeneous growth of conducting polymer nanofibers by electrodeposition for superhydrophobic and superoleophilic stainless steel meshes, RSC Adv. 4 (2014) 50401-50405.

[27] Spectral data were obtained from Wiley Subscription Services, Inc. (US), 2015 American Chemical Society.

[28] Spectral data were obtained from the National Institute of Advanced Industrial Science and Technology (Japan), 2015 American Chemical Society.

[29] R. Ryhage, E. Steuhagen, Mass spectrometry of organic ions, Academic Press (1963) 399-412.

[30] J. Wandass, J. Gardella, Secondary ion mass spectrometry of monomolecular layers of fatty acids prepared by Langmuir-Blodgett techniques, J. Am. Chem. Soc. 107 (1985) 6192-6195.

[31] B.P. Payne, M.C. Biesinger, N.S. McIntyre, Use of oxygen/nickel ratios in the XPS characterisation of oxide phases on nickel metal and nickel alloy surfaces, Journal of Electron Spectroscopy and Related Phenomena 185 (2012) 159–166.

[32] B.P. Payne, M.C. Biesinger, N.S. McIntyre, The study of polycrystalline nickel metal oxidation by water vapour, Journal of Electron Spectroscopy and Related Phenomena 175 (2009) 55–65.

[33] S. Oswald, W. Brückner, XPS depth profile analysis of non-stoichiometric NiO films, Surf. Interface Anal. 36 (2004) 17–22.

[34] H.W. Nesbitt, D. Legrand, G.M. Bancroft, Interpretation of Ni2p XPS spectra of Ni conductors and Ni insulators, Phys Chem Minerals 27 (2000) 357-366.

[35] S. Chehreh-Chelgani, B. Hart, M. Biesinger, J. Marois, M. Ourriban, Pyrochlore surface oxidation in relation to matrix Fe composition, Minerals Engineering 55 (2014) 165–171.

[36] Z. Chen, L. Hao, M. Duan, Electrodeposition fabrication of Co-based superhydrophobic powder coatings in non-aqueous electrolyte, Appl Phys A 111 (2013) 581-585.

## LIST OF FIGURE CAPTIONS

**Figure 1.** Contact angle at different electrolysis time. The standard deviation bars were included.

**Figure 2.** (a-c) SEM micrographs of 316L stainless steel superhydrophobic surface coatings for 30 sec (5). (d) The EDS spectrum of stainless steel superhydrophobic surface coatings for 30 s. Semi-quantitative composition of substrate and sample 5 in %wt are included.

**Figure 3.** SEM images of 316L stainless steel substrate and seven different conditions coated samples (1-7), a) sample 1 (900 s), b) sample 2 (600 s), c) sample 3 (300 s), d) sample 4 (60 s), e) sample 5 (30 s), f) sample 6 (20 s), g) sample 7 (15 s) and h) sample 8 (10 s).

**Figure 4.** AFM images of 316L stainless steel coated samples, 1- sample 1 (900 s), 2- sample 2 (600 s), 3- sample 3 (300 s), 4- sample 4 (60 s), 5- sample 5 (30 s), 6- sample 6 (20 s), 7- sample 7 (15 s). (1µm x 1µm study area)

**Figure 5.** AFM images of pillars in the superhydrophobic samples 6 (a) and 7 (b).

**Figure 6.** IR spectra of sample 1 (900 s), sample 2 (600 s), sample 3 (300 s), sample 4 (60 s), and sample 5 (30 s).

**Figure 7.** Secondary ion mass spectra of positive ions from sample 6 (20 s).

**Figure 8.** XPS spectra of 316L stainless steel coated samples, sample 1 (900 s), sample 2 (600 s), sample 3 (300 s), sample 4 (60 s), sample 5 (30 s), sample 6 (20 s), and sample 7 (15 s).

**Figure 9.** XPS spectra of deconvolution peaks of C (top) and O (bottom) of sample 1 and 5.

*Text Only in MS Word (Double-Spaced)
Click here to view linked References

# IDENTIFICATION OF THE MECHANISM THAT CONFERS SUPERHYDROPHOBICITY ON 316L STAINLESS STEEL

*Ana M. Escobar*[1], Nuria Llorca-Isern[1], Oriol Rius-Ayra[1]*

*corresponding author

[1] CPCM Departament de Ciència dels Materials i Enginyeria Metal·lurgica, Facultat de Química, Universitat de Barcelona, Marti-Franqués 1, 08028 Barcelona, Spain

ABSTRACT This study develops a rapid method to confer superhydrophobicity on 316L stainless steel surfaces with an amphiphilic reagent such as dodecanoic acid. The highest contact angle (approaching 173°) was obtained after forming hierarchical structures with a non-aqueous electrolyte by an electrolytic process. Our goal was to induce superhydrophobicity directly on 316 stainless steel substrates and to establish which molecules cause the effect. The superhydrophobic behaviour is analysed by contact angle measurements, scanning electron microscopy (SEM), IR spectroscopy and atomic force microscopy (AFM). The growth mechanism is analysed using FE-SEM, TOF-SIMS and XPS in order to determine the molecules involved in the reaction and the growth. The TOF-SIMS analysis revealed that the $Ni^{2+}$ ions react with lauric acid to create an ester on the stainless steel surface.

KEYWORDS Superhydrophobicity; stainless steel; coating; electrolytic reaction; self assembly; hierarchical structures.

## 1. INTRODUCTION

Superhydrophobic surfaces, with extremely high water contact angles (CAs) of more than 150° are of special interest due to their various anti-adhesive and self-cleaning properties [1]. A closely related phenomenon in nature is the lotus effect, which refer to surfaces that are difficult to wet. Recent studies demonstrate that the superhydrophobicity of lotus leaves principally results from the presence of binary structures at both the micrometer and nanometer scales together with the low-energy wax-like materials on the surfaces [2]. Materials with similar properties, to those of the lotus leaf structure are very useful in several areas, such as the aeronautical industry [3, 4] and civil engineering [5], so many methods have been developed to mimic the lotus leaf structure. Metals are very important and irreplaceable engineered materials in many industrial fields. Stainless steel is one of the most common metals or alloys; it is widely used in industry due its good mechanical workability and anticorrosion properties. Nevertheless, fabrication of superhydrophobic stainless steel has remained relatively unstudied compared to other metals such as zinc, copper or aluminium [6-10].

The wettability of solid substrates is known to be dependent on both their chemical composition and their topographic structure, either lowering the surface energy with different molecules [11, 12] or increasing surface roughness (through techniques such as sand-blasting [13] chemical etching [14] or grinding processes), reduces the affinity of water drops to the surface. Combining the appropriate surface roughness and low surface energy material leads to artificial superhydrophobic surfaces inspired by the lotus leaf [15], rose petal [16], leg of the water strider [17] and other natural surfaces with self-cleaning and water-repellent properties [18]. Until now, techniques to fabricate superhydrophobic stainless steel surfaces have been limited because they require special equipment, complex

processes or a considerable period of time; this is the case with the sol-gel process, chemical vapour deposition, laser treating and anodic oxidation [19-25]. Consequently, there is a need to develop a simple and rapid method for conferring superhydrophobicity on stainless steel surfaces, as could be envisaged through electrolytic coating at room temperature [26]. Here, in order to reduce the reaction time and simplify the procedure, we propose a two-step process: the initial step is to grind the 316L stainless steel surface to increase surface roughness, and the second, to reduce the surface energy of the substrate by electrodeposition of a metal-fatty acid. Superhydrophobicity is produced by the chemical reaction between nickel ions and lauric acid on a 316L stainless steel surface. The present study has three main objectives: to identify the molecules responsible for superhydrophobicity, the mechanism by which superhydrophobicity is produced, and consequently the influence of variables such as reaction time on the proposed processing method. We use time-of-flight secondary ion mass spectrometry (TOF-SIMS) and X-ray photoelectron spectroscopy (XPS) techniques to identify the molecules involved in the growth step, by paying close attention to the analysis of the mechanism by which the chemical reaction proceeds.

## 2. EXPERIMENTAL PROCEDURE

Pieces of commercial 316L stainless steel, 15 x 50 x 2 mm, were used as the substrate for this study. All the samples were produced by the same process, the details of which are as follows. First, the cleaned samples were ground with SiC abrasive paper ranging from an average particle diameter of 63 μm (P220 grade) to 15.3 μm “super fine” (P1200 grade). Second, the samples were ultrasonically cleaned with ethanol followed by deionized water and then, they were dried with forced air. Third, two cleaned samples were immersed

vertically into a uniform electrolyte solution of nickel chloride (0.05 M) and lauric acid (0.1 M) in ethanol, 3 cm apart: they were used as the cathode and the anode of an electrolyte cell, and a direct current (DC) voltage of 30 V was applied across the two electrodes. The etching time were modified from 900 to 10 seconds in order to evaluate the growth mechanism of the coating, until hydrophilic surfaces were obtained. After the selected electrolysis time, the working electrodes were immediately rinsed with ethanol and deionized water and dried in air, giving the as-prepared cathodic surface. Consecutive numbers were assigned to the samples in order to identify each electrolysis condition with its corresponding sample; the surface produced after 900 seconds of electrolysis was numbered 1 and the rest of the specimens were numbered following the descending order of electrolysis times as shown in Table 1.

Table 1. Electrolysis time for the different set of samples.

| **Sample** | **1** | **2** | **3** | **4** | **5** | **6** | **7** | **8** |
|---|---|---|---|---|---|---|---|---|
| **Electrolysis time/ s** | 900 | 600 | 300 | 60 | 30 | 20 | 15 | 10 |

The specimen surface was characterized using a Hitachi S-4100 field emission scanning electron microscope (FE-SEM) in order to study their morphological features. Atomic force microscopy (AFM) measurements were taken using a Dimension 3100 microscope attached to Nanoscope IV electronics (Bruker) using Si probes with a nominal spring constant of 40 nN/nm (T300R-W, Vistaprobes). All the topographic measurements were performed in tapping mode at a scan rate of 0.3Hz and 512x512 pixels resolution. The samples were imaged in air and at 55% RH. The AFM measurements were carried out in Peak Force Scan

Asyst mode (QNM) in order to quantify the Young's modulus of the surfaces. The initial roughness was measured by confocal microscopy using LeicaScan DCM 3D on a surface of 1.21x 0.91 mm. The reported roughness values are the average of three measurements at different places on the surface. The chemical groups of the superhydrophobic coatings were determined by infrared absorption spectroscopy (Thermo Scientific Nicolet IN10MX). The chemical composition of the surface was analysed by X-ray photoelectron spectroscopy in a PHI 5500 Multitechnique System (Physical Electronics) with a monochromatic X-ray source (Aluminium Kα line of 1486.6 eV and 350 W) on 0.8 mm diameter discs. All measurements were made in an ultra-high vacuum (UHV) chamber pressure between $5x10^{-9}$ and $2x10^{-8}$ torr. The carbon 1s line was used to calibrate the binding-energy scale for XPS measurements, for which a binding energy of 284.8 eV was assumed. High-resolution mass spectra of positive and negative secondary ions were obtained using TOF-SIMS IV (ION-TOF, Munster, Germany) equipment operating at a pressure of $5 \times 10^{-9}$ mbar with a 25 keV pulsed bismuth liquid metal ion source ($Bi_3^{++}$). Secondary ions were detected with a reflector TOF analyser, multichannel plates (MCPs), and a time-to-digital converter (TDC). Measurements were performed with a typical acquisition time of 10 s, at a TDC time resolution of 200 ps and a 100 µs cycle time. Secondary ion spectra were acquired from randomly rastered sample surface areas of 100 x 100 µm. Mass spectral acquisition was performed using the ION-TOF Ion Spec software (version 4.1). Finally, CA were measured with a Contact Angle Measuring System DSA 100 from KRÜSS with 10 µL of deionized water at room temperature. The reported CA values are the average of three measurements of CA of droplets at different places on the surface. Sliding angles were measured by dropping a water droplet on a superhydrophobic sample positioned on a tilting stage. The tilting angle of the stage was adjusted using a micrometer with a resolution of 0.5°. Sliding

angles values are the average of three measurements of droplets at different places on the surface, the standard deviation were calculated and it is minor than 1° in all the measured samples.

## 3. RESULTS AND DISCUSSION

Samples were prepared using the procedure outlined above. In order to produce superhydrophobic surfaces on 316L stainless steel, we reduced the electrolysis time from 900 seconds down to the minimum necessary to produce a hydrophilic surface, using the same materials and coating method. An electrolysis time of 10 seconds was enough to generate hydrophilic stainless steel. The growth mechanism of the coating was thus studied.

Surface wettability was evaluated by static CA measurements of hydrophobic samples and the 316L stainless steel substrate. As shown in Figure 1, there is no obvious correlation between electrolysis time and hydrophobic effect in this experiment. The highest CA was 175° at 30 seconds (sample 5) with a sliding angle of 3.5° and the lowest CA was 160° at both 20 s (sample 6) and 600 seconds (sample 2) with sliding angles of 5° and 4.5°, respectively. The 316L stainless steel substrate had hydrophilic properties with a CA of 40°. In summary, the procedure to make a superhydrophobic surface does not need much time: 30 seconds of electrolysis time was sufficient to achieve maximum superhydrophobicity.

Figure 2 shows the typical morphology of the surface after 30 seconds of electrolysis (sample 5); top right, top left and bottom left are the SEM micrographs with low and high magnification, respectively. It can clearly be seen that the surface of 316L stainless steel is textured with 2 μm pillars along the grinding direction. In greater detail, we can also observe that the surfaces of the pillars are covered by nanoscale granular protrusions. These

hierarchical micro-nano structures have grooves that trap a fraction of the air, thereby favouring the hydrophobicity of the material. The EDS spectrum (Fig. 2d), suggests that the composition of the coating is mostly Ni and O.

Figure 3 (a-h) shows the surface morphology of the samples 1 to 8 after different electrolysis times. The microstructure of all the surfaces is formed mainly of pillars and islands. Surfaces 1, 2 and 3 (900, 600 and 300 seconds of electrolysis, respectively) are completely coated and mainly formed of islands; whereas surfaces with shorter electrolysis times (samples 4, 5, 6 and 7) are only partially covered, showing that the coating initially generates pillars, which suggests a process related to the Volmert-Weber growth mode, as can be observed in some areas of the substrate. The surface of sample 8 has widely dispersed pillars (Fig. 3h), this sample is not superhydrophobic. Bubble-like protuberances with different diameters between 2 and 5 μm are observed on all the samples.

From the mechanism point of view, the building block is the pillar, followed by the island formation which is a connected group of pillars. It is not necessary that both cover the entire surface for producing superhydrophobicity.

AFM images (1 x 1 $\mu m^2$ area) were produced to compare the final roughness of the superhydrophobic specimens using RMS roughness as a comparison parameter; and also to calculate their Young's modulus. Both results are summarized in Table 2.

Table 2. RMS and E from AFM analysis of coated samples.

| **Sample** | **Prepared substrate** | **1** | **2** | **3** | **4** | **5** | **6** | **7** |
|---|---|---|---|---|---|---|---|---|
| **RMS/nm** | 210 | 55 | 20 | 12 | 45 | 39 | 124 | 189 |
| **E/GPa** | 200 | 0.20 | 0.5 | 0.25 | 0.58 | 0.41 | 0.29 | 0.04 |

The AFM images are shown in Figure 4. The surface roughness resulting from the AFM analysis of the coated samples indicates that the highest RMS value corresponds to the sample that underwent the least electrolysis time. This can be explained by the treatment only generating pillars without connections between them. In contrast, samples that underwent longer electrolysis times have neighbouring pillars connected, forming a more homogeneous surface with less roughness. These results are consistent with our FE-SEM analysis. The Young's modulus values are very low due to the organic nature of the coating, compared to the substrate AISI 316L modulus (200 GPa).

AFM analysis allowed us to measure the width of the pillars in the initial step of the growth mechanism on the samples that underwent the shortest electrolysis time. Figure 5 shows the surface of sample 6 with vertical distance values between 104 and 146 nm; whereas the surface of sample 7 has vertical distance of 70 to 212 nm. In accordance with these results, it can be concluded that 70-100 nm is the minimum height of pillars necessary to obtain superhydrophobic 316L stainless steel using a lauric acid-nickel chloride-ethanol medium.

The SEM and AFM analysis confirmed that the coating starts with the formation of pillars, then, the islands morphology results when several pillars grow together. Finally the surface of the sample is completely covered (as shown after 300 seconds of electrolysis).

In order to confirm the chemical composition of the as-prepared coatings, IR, TOF-SIMS and XPS techniques were used. Figure 6 shows IR spectra of the as-prepared coatings (the samples with the shortest electrolysis times (samples 6 and 7) were not observed by this technique). The IR spectra indicate that the free acidic group band from the lauric acid at 1702 $cm^{-1}$ is no longer present, compared to the MICC-73396-421X spectrum (CAS

registry number 143-07-7, CAS index name dodecanoic acid) [27], whereas the peak at 1590 $cm^{-1}$ corresponding to coordinated ester groups appears as in the NIDA71076 spectrum (CAS registry number 13282-11-6, CAS index name dodecanoic acid, $nickel^{2+}$ salt (2:1)) [28]. Therefore, it can be concluded that $(CH_3(CH_2)_{10}COOH$ changed into $(CH_3(CH_2)_{10}COO^-$. The two peaks at 2850 and 2922 $cm^{-1}$ belong to the symmetric and asymmetric C-H stretching modes of the $CH_2$ groups of laureate, respectively. This supports the previous finding.

TOF-SIMS was used to study the chemical reactions and lateral distributions of fatty acids enhanced to react on 316L stainless steel surfaces. On these alloy surfaces, a direct interaction between the acid and nickel ions is observed via detection of a molecular ion that corresponds to the mass of the laureate anion, nickel cation and $Ni[laureate]_2$. Since TOF-SIMS can detect and discriminate specific chemical reaction products, it was used to identify reaction products formed between the fatty acid molecules, nickel ions and metallic surface. The positive secondary ion mass spectra for sample 6 (20 s of electrolysis is shown at Fig. 7. The assignments are based upon classical mass spectroscopic fragmentation patterns [29]. Wandass et all, [30] studied different fatty acids on silver surfaces using TOF-SIMS, including lauric acid and they obtained similar signals to those obtained in our study. The peaks represent masses of: 100 units, which corresponds to $(CH_2CONi)^+$; 133 units, for $(CH_3CH_2COONi)$; 266 units, for $Na(CH_3(CH_2)_9COONi)^+$, (Na is considered a contaminant that is easily detected by SIMS); and 411 units, for $(CH_3(CH_2)_{10}COO\text{-}Ni\text{-}OOC(CH_2)_{10}CH_3$ + $H\text{-}HCOOH)^+$. The presence of these species on the stainless steel surface was also confirmed by the XPS Ni 2p and O 2s signals.

XPS was used to characterize the coating on the 316L stainless steel and to determine its composition. We analysed all seven samples from 15 to 900 s of electrolysis, considering oxygen, carbon and nickel peaks. In all the samples, the peaks were repeated at the same value of the binding energy. Figure 8 shows the superhydrophobic sample spectra. The peak at 852 eV is attributed to Ni metal; its intensity decreases as the process time increases because after less than 30 seconds of electrolysis the coating is thicker after more than 60 seconds of electrolysis. After less than 30 seconds, XPS detected Ni metal from the substrate and also Ni metal in the coating; in contrast to the results after more than 60 seconds of electrolysis, when XPS mostly detected Ni metal formed by the reaction.

Figure 9 shows two examples of C (top) and O (bottom) deconvolution corresponding to sample 5 and sample 1. The peak located at 284.6 eV is attributed to C-1s and its deconvolution gives three peaks: the first is located at 288 eV and it is attributed to the carbonyl of lauric acid [31, 32]; the second is at 286 eV corresponding to the ester group [32]; while the third is at 284 eV and it is attributed to adventitious carbon [32] (Fig. 9top). The peak located at 531.7 eV is attributed to O-2s and its deconvolution also gives three peaks; the binding energy of the first is 529 eV and it is attributed to NiO; the second is located at 531 eV and it is attributed to $Ni(OH)_2$; and the last located at 532 eV is attributed to the C-O bond [33] (Fig 9bottom). The peak located at 856.5 eV is attributed to Ni-$2p_{3/2.}$ Its deconvolution again gives three new peaks; the first located at 852 eV is attributed to Ni metal; the second at 856 eV is attributed to $Ni(OH)_2$; and the last at 861 eV is attributed to a satellite of the previous compound and so it also corresponds to $Ni(OH)_2$ [34]. Finally, the peak located at 711 eV corresponds to the Fe-$2p_{3/2}$ from the stainless steel substrate. [35]

The XPS results reveal the presence of metallic nickel and also oxidized nickel corresponding to the $Ni[CH_3(CH_2)_{10}COO)]_2$ molecule. A similar product was also observed

by Chen et al [36] in their research on cobalt-based coatings using X ray diffraction techniques. In the present study, the TOF-SIMS results confirm the bonding between lauric acid and Ni, as well as the existence of metallic nickel.

One factor that promotes superhydrophobicity can be attributed to the chemical composition of the surface on which superhydrophobicity will appear. A chemical reaction will be associated with each part of the process that produces the change to superhydrophobicity of the 316L stainless steel surface. Based on our XPS and TOF-SIMS analysis, the proposed reaction mechanism for the as-prepared superhydrophobic coatings involves the $Ni^{2+}$ ions around the cathode plate being reduced to metallic nickel on the cathodic surface when the voltage is applied across the two 316L stainless steel electrodes. The metallic nickel will then act as growth sites. Meanwhile, more $Ni^{2+}$ ions near the cathodic plate will react with the lauric acid and form nickel laureate on the activated surface of the 316L stainless steel. The reaction processes can be formulated as follows:

**Scheme 1.** Redox reaction

$$Fe_{(s)} \rightarrow Fe_{(aq)}^{2+} + 2\,\bar{e}$$

$$Ni_{(aq)}^{2+} + 2\bar{e} \rightarrow Ni_{(s)}\,(\text{growth site})$$

**Scheme 2.** Laureate formation

$$Ni_{(aq)}^{2+} + CH_3(CH_2)_{10}COOH_{(aq)} \rightarrow Ni[CH_3(CH_2)_{10}COO]_2 + 2H_{(aq)}^{+}$$

## 4. CONCLUSIONS

Superhydrophobic surfaces on 316L stainless steel were developed via a short procedure consisting of the electrolysis of stainless steel in the lauric/nickelchloride/ethanol

electrolyte. 30 seconds of reaction was enough to obtain an optimum superhydrophobic 316L stainless steel surface (CA 175°).

Reducing the electrolysis time allowed us to identify the growth mechanism as three-dimensional islands (Volmert-Weber mode) thus leading to the superhydrophobicity via simultaneous pillar growth. Consequently, from the mechanism point of view, the building block is the pillar, followed by the island formation which is a connected group of pillars. Experimentally it is found that it is not necessary that both cover the entire surface for producing superhydrophobic character.

From the property point of view, the characteristic magnitude seems to be the vertical height of the pillars and the islands for producing superhydrophobicity. We used AFM to stablish the minimum range of vertical height of the pillars necessary to obtain superhydrophobic 316L stainless steel.

TOF-SIMS and XPS analysis allowed us to identify the species responsible for the superhydrophobicity on the 316L stainless steel substrate as $CH_3(CH_2)_{10}COONiOH$ and $(CH_3(CH_2)_{10}COO)_2Ni$.

Superhydrophobicity is associated to the redox reaction of $Fe/Ni^{2+}$ to $Fe^{2+}/Ni$, with Ni as the growth site, and also with the laureate formation reaction.

## 5. REFERENCES

[1] B. Bhushan, Y.C. Jung, Natural and biomimetic artificial surfaces for superhydrophobicity, self-cleaning, low adhesion, and drag reduction, Prog. Mater. Sci. 56 (2011) 1-108.

[2] N. Valipour, F. Ch. Birjandi, J. Sargolzaei, Super-non-wettable surfaces: A review, Colloids and Surfaces A: Physicochem. Eng. Aspects 448 (2014) 93-106.

[3] J. Ou,W. Hu, M. Xue, F. Wang, W. Li, Superhydrophobic surfaces on light alloy substrates fabricated by a versatile process and their corrosion protection, ACS Appl. Mater. Interfaces 5 (2013) 3101-3107.

[4] J. Xiao, S. Chaudhuri, Design of anti-icing coatings using supercooled droplets as nano-to-microscale probes, Langmuir 28 (2012) 4434-4446.

[5] Y. Huang, D.K. Sarkar, D. Gallant, X-Grant Chen, Corrosion resistance properties of superhydrophobic copper surfaces fabricated by one-step electrochemical modification process, App. Surf. Sci. 282 (2013) 689-694.

[6] Y. Wan, Z. Wang, Z. Xu, C. Liu, J. Zhang, Fabrication and wear protection performance of superhydrophobic surface on zinc, App. Surf. Sci. 257 (2011), 7486-7489.

[7] P. Li, X. Chen, G. Yang, L. Yu, P. Zhang, Preparation of silver-cuprous oxide/stearic acid composite coating with superhydrophobicity on copper substrate and evaluation of its friction-reducing and anticorrosion abilities, App. Surf. Sci. 289 (2014) 21-26.

[8] A. M. Escobar, N. Llorca-Isern, Superhydrophobic coating deposited directly on aluminium, App. Surf. Sci. 305 (2014) 774-782.

[9] J. Ou, W. Hu, M. Xue, F. Wang, W. Li, One-step solution immersion process to fabricate superhydrophobic surfaces on light alloys, ACS Appl. Mater. Interfaces 5 (2013) 9867-9871.

[10] X. Zhu, Z. Zhang, X. Men, J. Yang, K. Wang, X. Xu, X. Zhou, Robust superhydrophobic surfaces with mechanical durability and easy repairability, J. Mater. Chem (2011), DOI:10.1039/c1jm12513.

[11] A. Nouri, C. Wen, Surfactants in mechanical alloying/milling: a catch-22 situation, Critical Reviews in solid state and materials Sciences 39 (2014) 81-108.

[12] L. Boinovich, A. Emelyanenko, V. Ivanov, A. Pashinin, Durable icephobic coating for stainless steel, ACS Appl. Mater. Interfaces 5 (2013) 2549-2554.

[13] M. Frank, A. Boccaccini, S. Virtanen, A facile and scalable method to produce superhydrophobic stainless steel surface, Appl. Surf. Sci. 311 (2014) 753-757.

[14] L. Li, V. Breedveld, D. Hess, Creation of superhydrophobic stainless steel surfaces by acid treatments and hydrophobic film deposition, ACS Appl. Mater. Interfaces 4 (2012) 4549-4556.

[15] L. Chen, Z. Xiao, P. Chan, Y. Lee, Static and dynamic characterization of robust superhydrophobic surfaces built from nano-flowers on silicon micro-post arrays, J. Micromech. Microeng. 20 (2010) 105001.

[16] Y. Liu, J. Liu, S. Li, Z. Han, Fabrication of biomimetic super-hydrophobic surface on aluminum alloy, J. Mater Sci. 49 (2014) 1624-1629.

[17] D. Hu, B. Chan, J. Bush, The hydrodynamics of water strider locomotion, Nature 424 (2003) 663-666.

[18] Y. Zhang, Q. Chen, E. Kim, H. Sun, Biomimetic grapheme films and their properties, Nanoscale 4 (2012) 4858-4869.

[19] Y. Yan, N. Gao, W. Barthlott, Mimicking natural superhydrophobic surfaces and grasping the wetting process: a review on recent progress in preparing superhydrophobic surfaces, Advanced in Colloid and Interface Science 169 (2011) 80-105.

[20] M. Kavale, S. Mahadik, D. Mahadik, V. Parale, A. Rao, R. Vhatkar, P. Wagh, S. Gupta, Enrichment in hydrophobicity and scratch resistant properties of silica films on glass by grafted microporosity of the network, J. Sol-Gel Sci. Technol. 64 (2012) 9-16.

[21] K. Ellinas, S. Pujari, D. Dragatogiannis, C. Chariditis, A. Tserepi, H. Zuilhof, E. Gogolides, Plasma micro-nanotextured, scratch, water and hexadecane resistant, superhydrophobic and superamphiphobic polymeric surfaces with prefluorinated monolayers, ACS Appl. Mater. Interfaces 6 (2014) 6510-6524.

[22] A. Leon, R. Pernites, R. Advincula, Superhydrophobic colloidally textured polythiophene film as superior anticorrosion coating, ACS Appl. Mater. Interfaces 4 (2012) 3169-3176.

[23] F.J. Wang, S. Lei, J.F. Ou, M.S. Xue, W. Li, Superhydrophobic surfaces with excellent mechanical durability and easy repairability, Appl. Surf. Sci. 276 (2013) 397-400.

[24] C. Badre, P. Dubot, D. Lincot, T. Pauporte, M. Turmine, Effects of nanorod structure and conformation of fatty acid self-assembled layers on superhydrophobicity of zinc oxide surface, J. Colloid Interface Sci. 316 (2007) 233-237.

[25] D. Ebert, B. Bhushan, Durable lotus-effect surfaces with hierarchical structure using micro- and nanosized hydrophobic silica particles, J. Colloid Interface Sci. 368 (2012) 584-591.

[26] T. Darmanin, F. Guittard, Homogeneous growth of conducting polymer nanofibers by electrodeposition for superhydrophobic and superoleophilic stainless steel meshes, RSC Adv. 4 (2014) 50401-50405.

[27] Spectral data were obtained from Wiley Subscription Services, Inc. (US), 2015 American Chemical Society.

[28] Spectral data were obtained from the National Institute of Advanced Industrial Science and Technology (Japan), 2015 American Chemical Society.

[29] R. Ryhage, E. Steuhagen, Mass spectrometry of organic ions, Academic Press (1963) 399-412.

[30] J. Wandass, J. Gardella, Secondary ion mass spectrometry of monomolecular layers of fatty acids prepared by Langmuir-Blodgett techniques, J. Am. Chem. Soc. 107 (1985) 6192-6195.

[31] B.P. Payne, M.C. Biesinger, N.S. McIntyre, Use of oxygen/nickel ratios in the XPS characterisation of oxide phases on nickel metal and nickel alloy surfaces, Journal of Electron Spectroscopy and Related Phenomena 185 (2012) 159–166.

[32] B.P. Payne, M.C. Biesinger, N.S. McIntyre, The study of polycrystalline nickel metal oxidation by water vapour, Journal of Electron Spectroscopy and Related Phenomena 175 (2009) 55–65.

[33] S. Oswald, W. Brückner, XPS depth profile analysis of non-stoichiometric NiO films, Surf. Interface Anal. 36 (2004) 17–22.

[34] H.W. Nesbitt, D. Legrand, G.M. Bancroft, Interpretation of Ni2p XPS spectra of Ni conductors and Ni insulators, Phys Chem Minerals 27 (2000) 357-366.

[35] S. Chehreh-Chelgani, B. Hart, M. Biesinger, J. Marois, M. Ourriban, Pyrochlore surface oxidation in relation to matrix Fe composition, Minerals Engineering 55 (2014) 165–171.

[36] Z. Chen, L. Hao, M. Duan, Electrodeposition fabrication of Co-based superhydrophobic powder coatings in non-aqueous electrolyte, Appl Phys A 111 (2013) 581-585.

## LIST OF FIGURE CAPTIONS

**Figure 1.** Contact angle at different electrolysis time. The standard deviation bars were included.

**Figure 2.** (a-c) SEM micrographs of 316L stainless steel superhydrophobic surface coatings for 30 sec (5). (d) The EDS spectrum of stainless steel superhydrophobic surface coatings for 30 s. Semi-quantitative composition of substrate and sample 5 in %wt are included.

**Figure 3.** SEM images of 316L stainless steel substrate and seven different conditions coated samples (1-7), a) sample 1 (900 s), b) sample 2 (600 s), c) sample 3 (300 s), d) sample 4 (60 s), e) sample 5 (30 s), f) sample 6 (20 s), g) sample 7 (15 s) and h) sample 8 (10 s).

**Figure 4.** AFM images of 316L stainless steel coated samples, 1- sample 1 (900 s), 2- sample 2 (600 s), 3- sample 3 (300 s), 4- sample 4 (60 s), 5- sample 5 (30 s), 6- sample 6 (20 s), 7- sample 7 (15 s). (1µm x 1µm study area)

**Figure 5.** AFM images of pillars in the superhydrophobic samples 6 (a) and 7 (b).

**Figure 6.** IR spectra of sample 1 (900 s), sample 2 (600 s), sample 3 (300 s), sample 4 (60 s), and sample 5 (30 s).

**Figure 7.** Secondary ion mass spectra of positive ions from sample 6 (20 s).

**Figure 8.** XPS spectra of 316L stainless steel coated samples, sample 1 (900 s), sample 2 (600 s), sample 3 (300 s), sample 4 (60 s), sample 5 (30 s), sample 6 (20 s), and sample 7 (15 s).

**Figure 9.** XPS spectra of deconvolution peaks of C (top) and O (bottom) of sample 1 and 5.

**Table(s)**

Table 1. Electrolysis time for the different set of samples.

| **Sample** | **1** | **2** | **3** | **4** | **5** | **6** | **7** | **8** |
|---|---|---|---|---|---|---|---|---|
| **Electrolysis time/ s** | 900 | 600 | 300 | 60 | 30 | 20 | 15 | 10 |

Table 2. RMS and E from AFM analysis of coated samples.

| Sample | Prepared substrate | 1 | 2 | 3 | 4 | 5 | 6 | 7 |
|---|---|---|---|---|---|---|---|---|
| **RMS/nm** | 210 | 55 | 20 | 12 | 45 | 39 | 124 | 189 |
| **E/GPa** | 200 | 0.20 | 0.5 | 0.25 | 0.58 | 0.41 | 0.29 | 0.04 |

**High-resolution Figure(s)**
**Click here to download high resolution image**

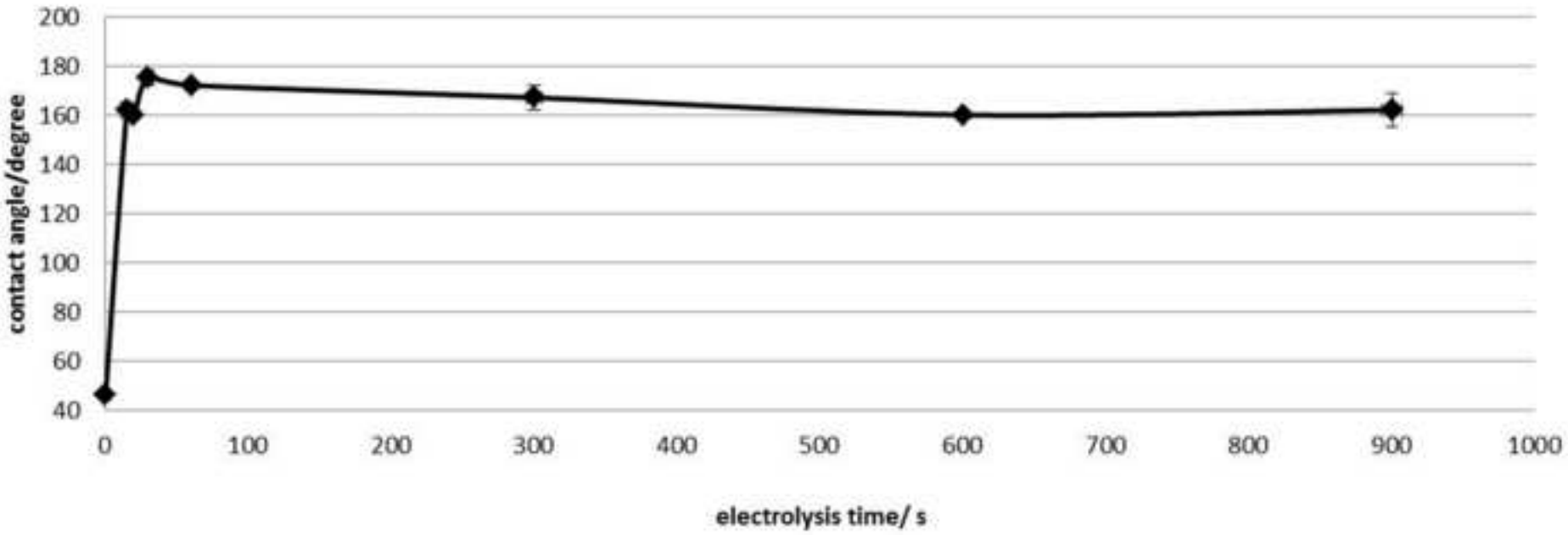

**High-resolution Figure(s)**

**Click here to download high resolution image**

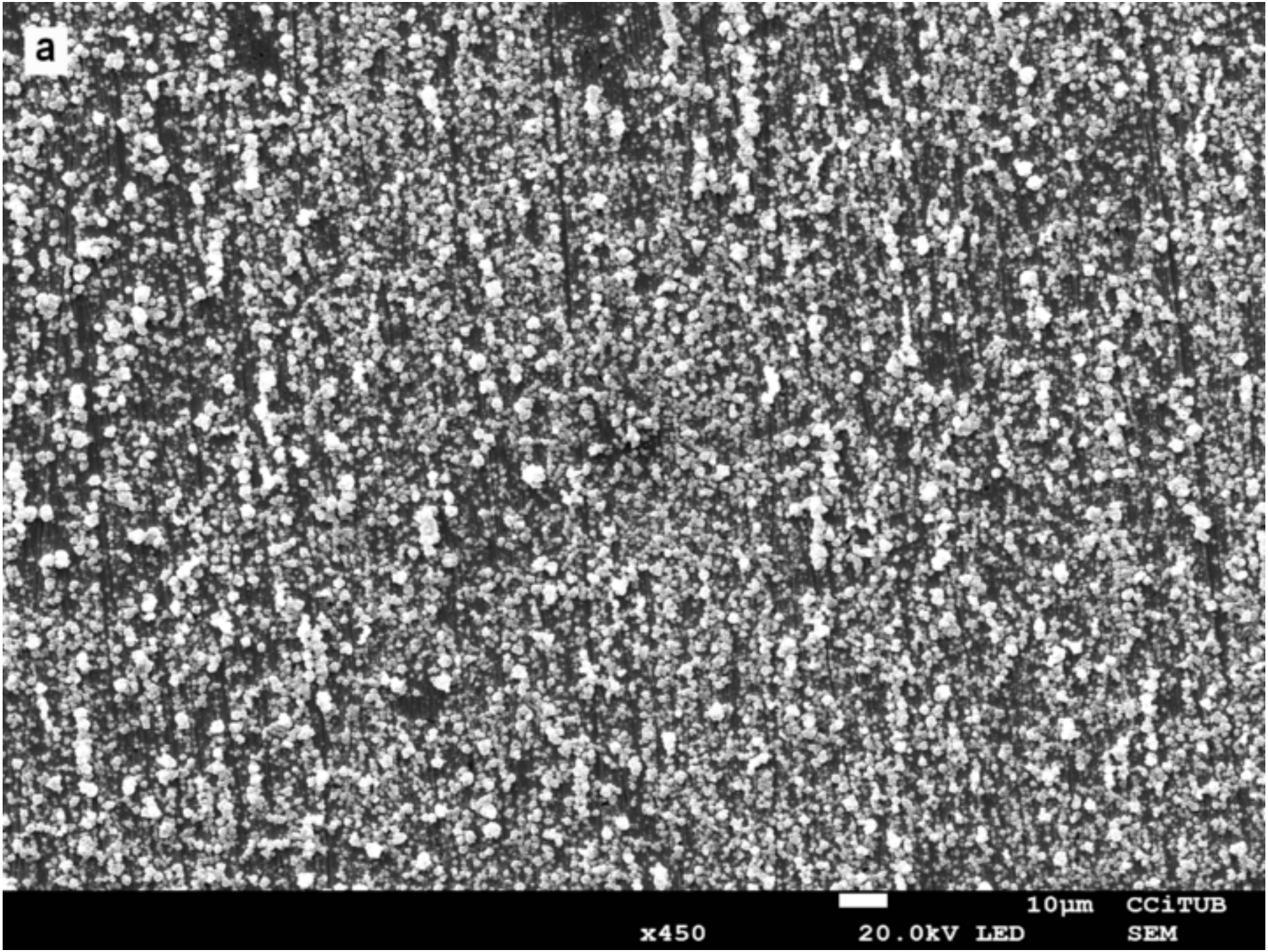

**High-resolution Figure(s)**
**Click here to download high resolution image**

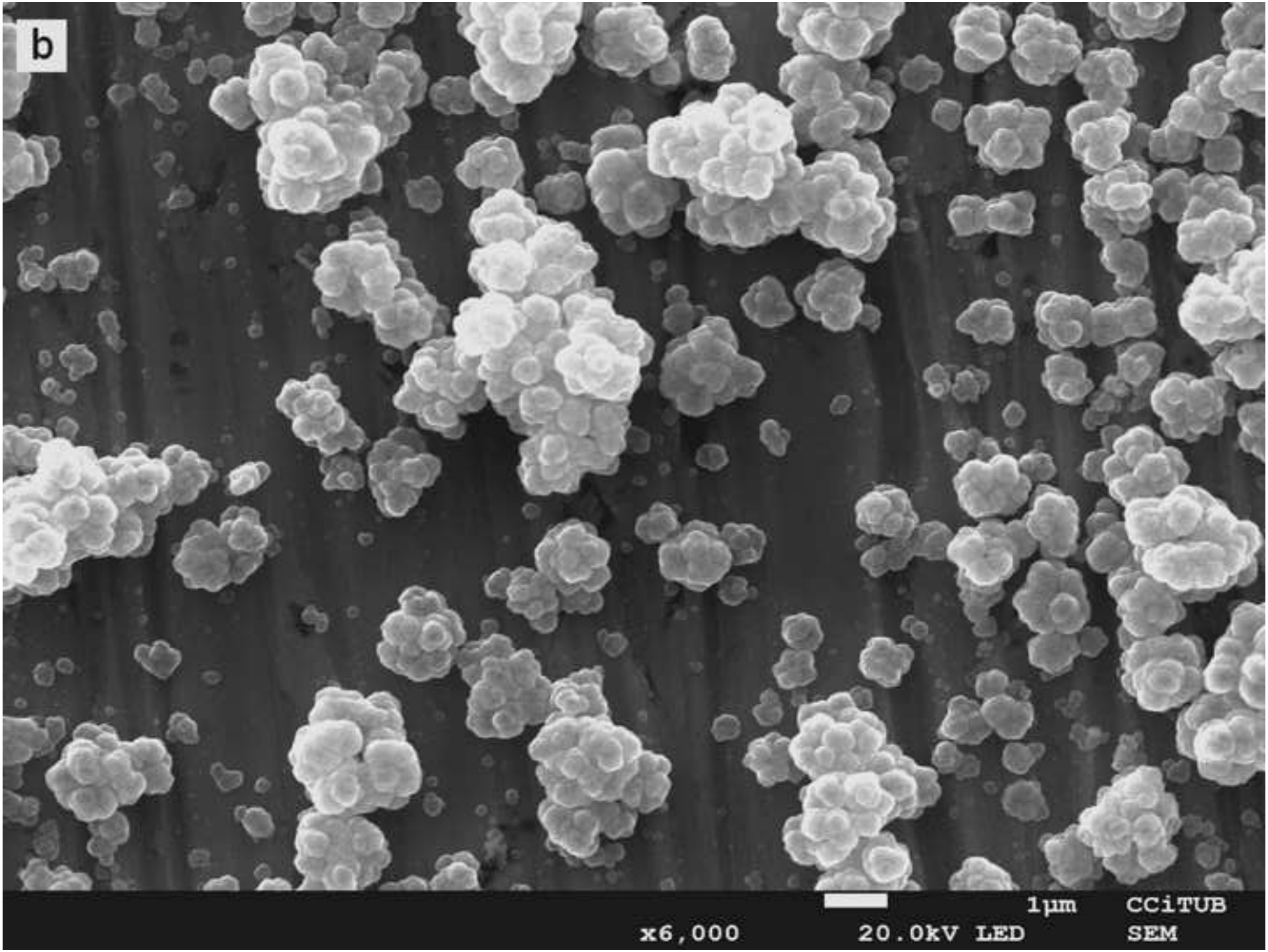

**High-resolution Figure(s)**

**Click here to download high resolution image**

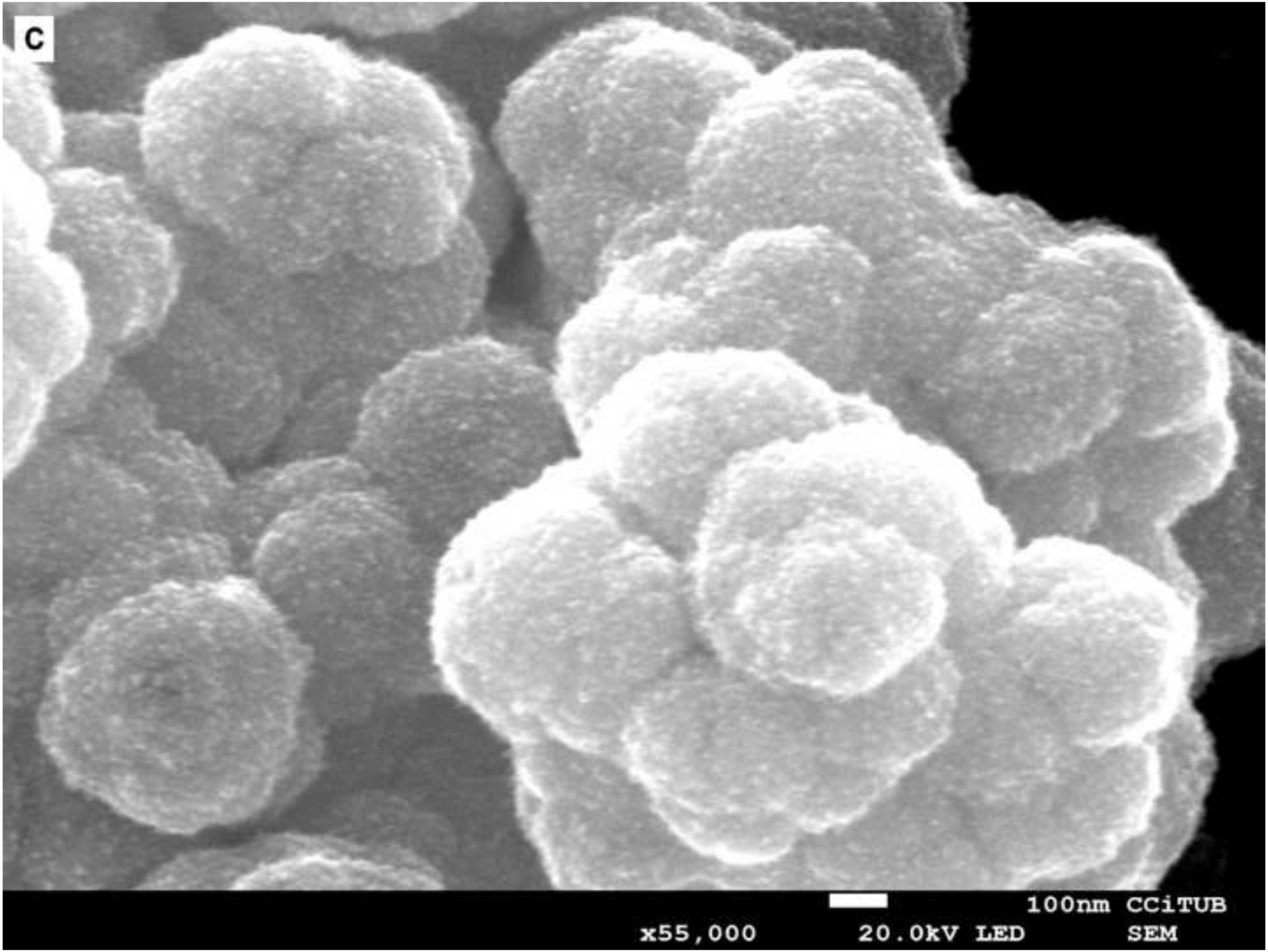

**High-resolution Figure(s)**
**Click here to download high resolution image**

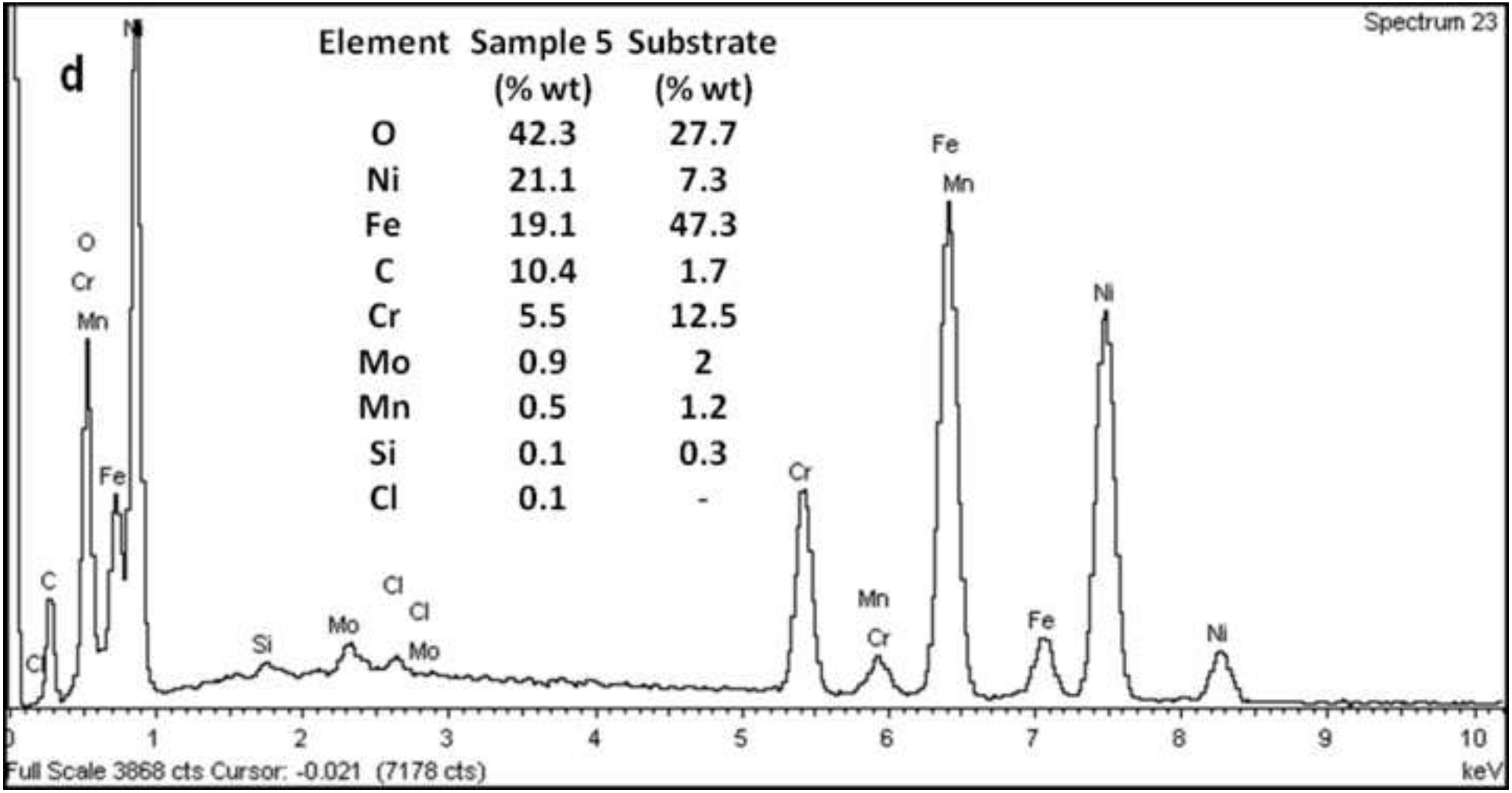

**High-resolution Figure(s)**

**Click here to download high resolution image**

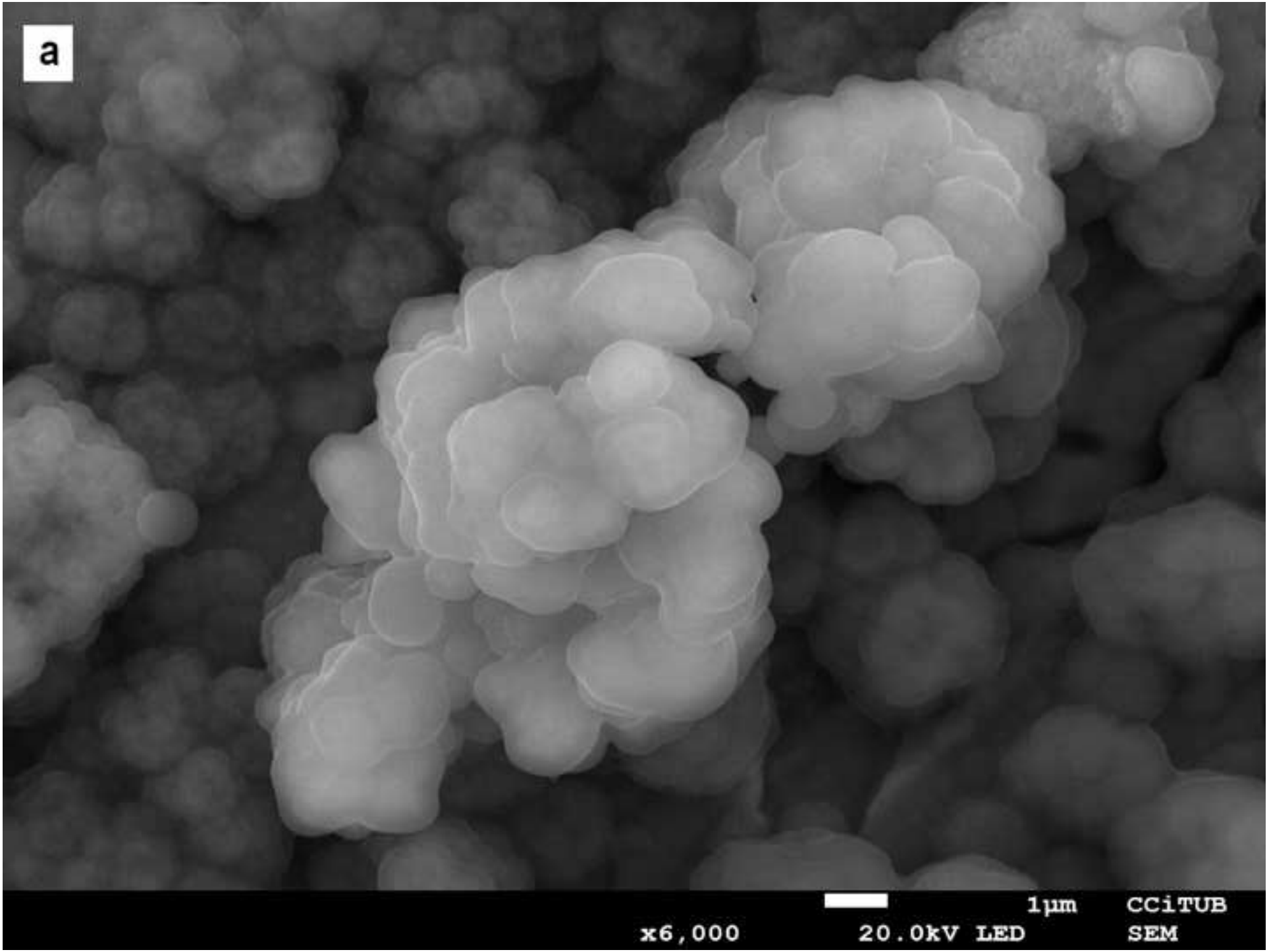

**High-resolution Figure(s)**

**Click here to download high resolution image**

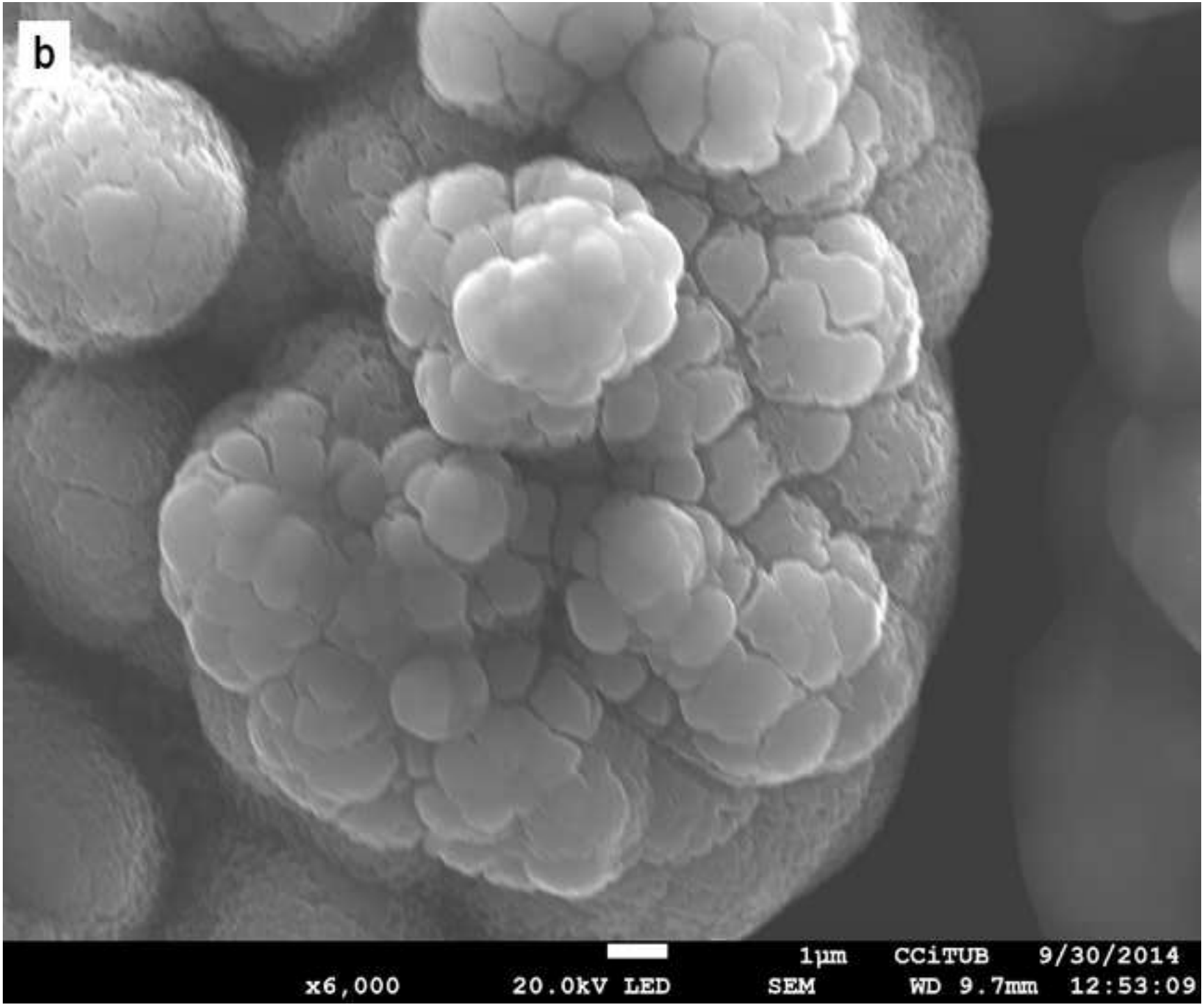

**High-resolution Figure(s)**

**Click here to download high resolution image**

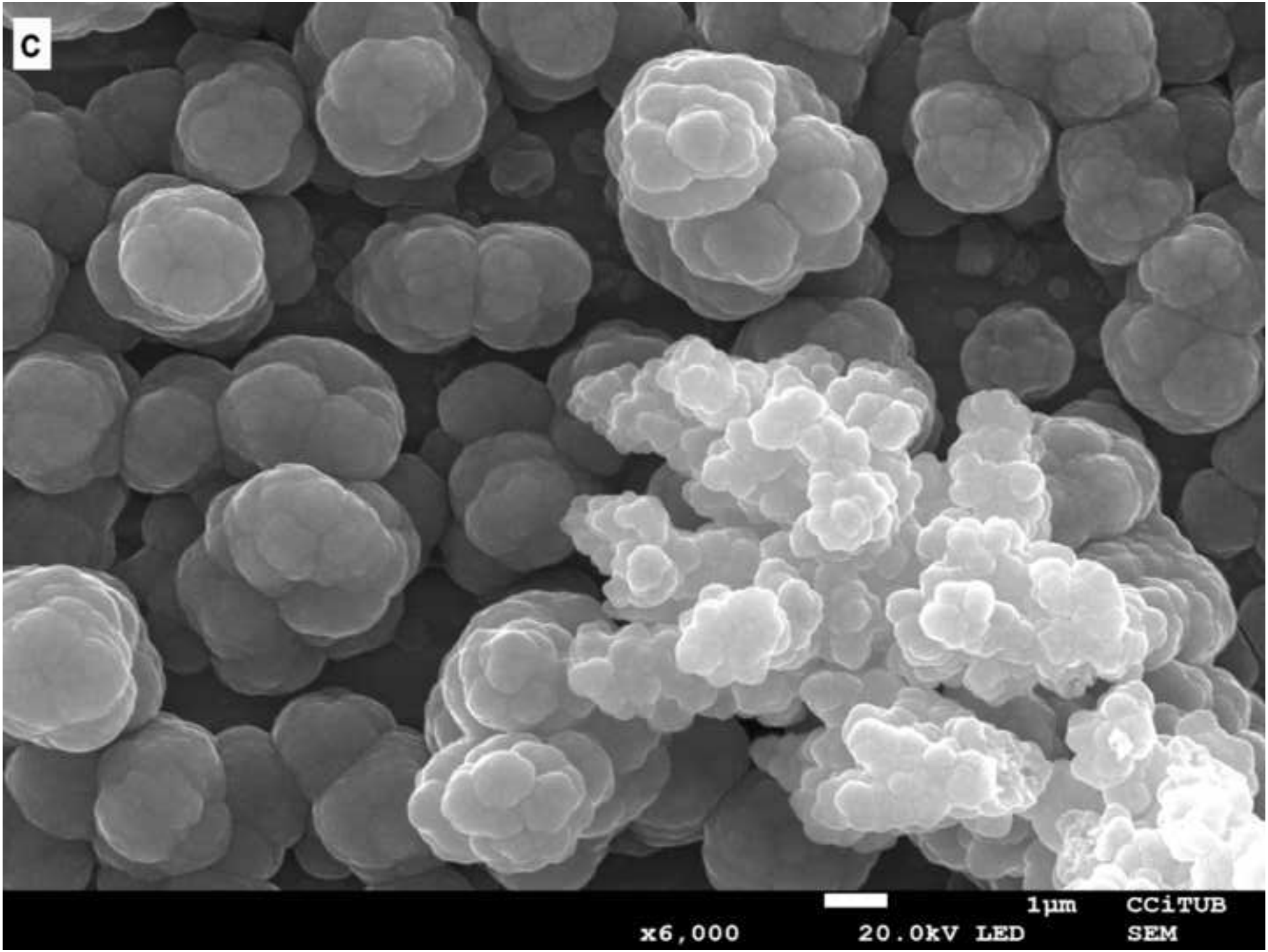

**High-resolution Figure(s)**

**Click here to download high resolution image**

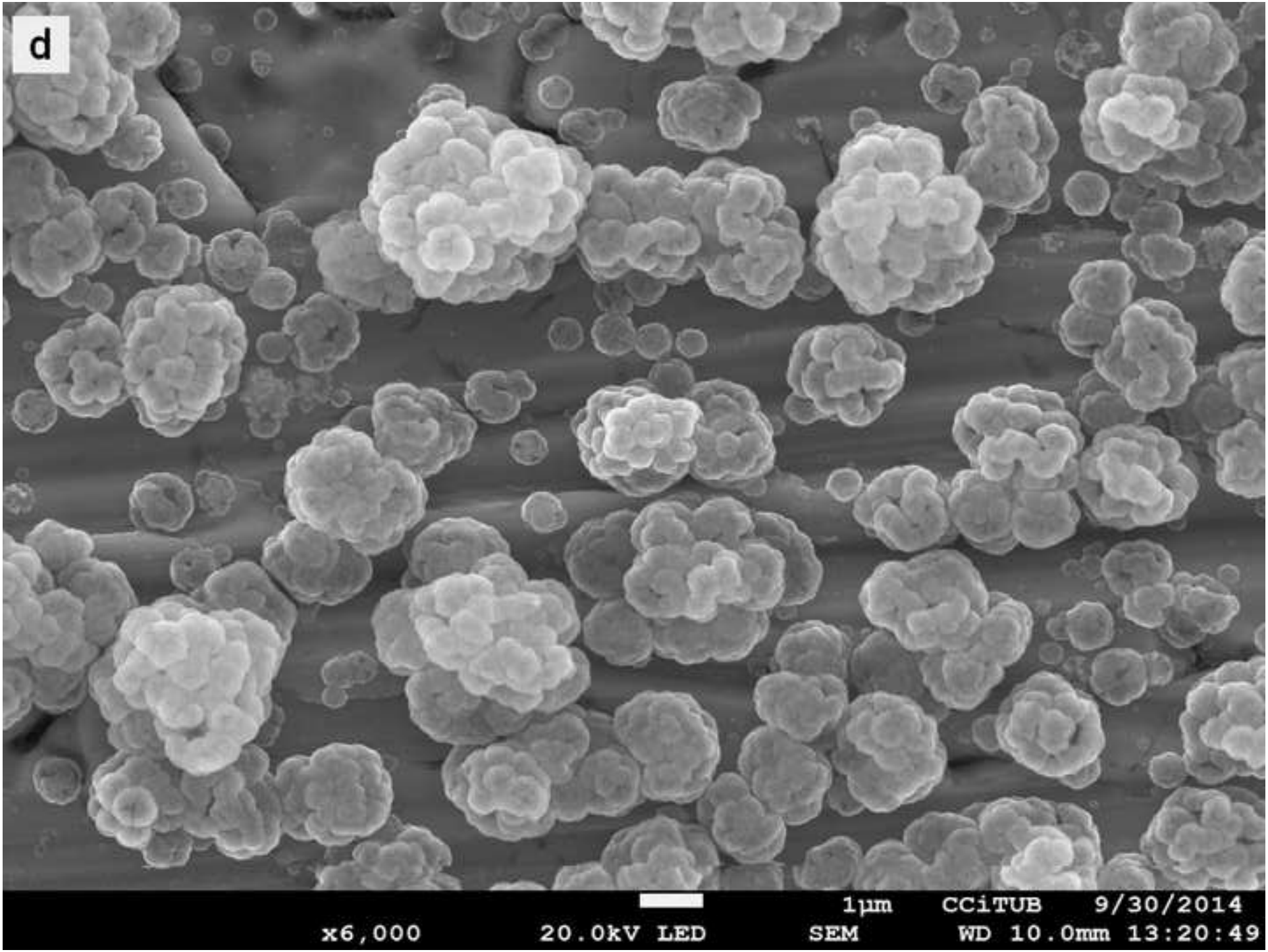

**High-resolution Figure(s)**
**Click here to download high resolution image**

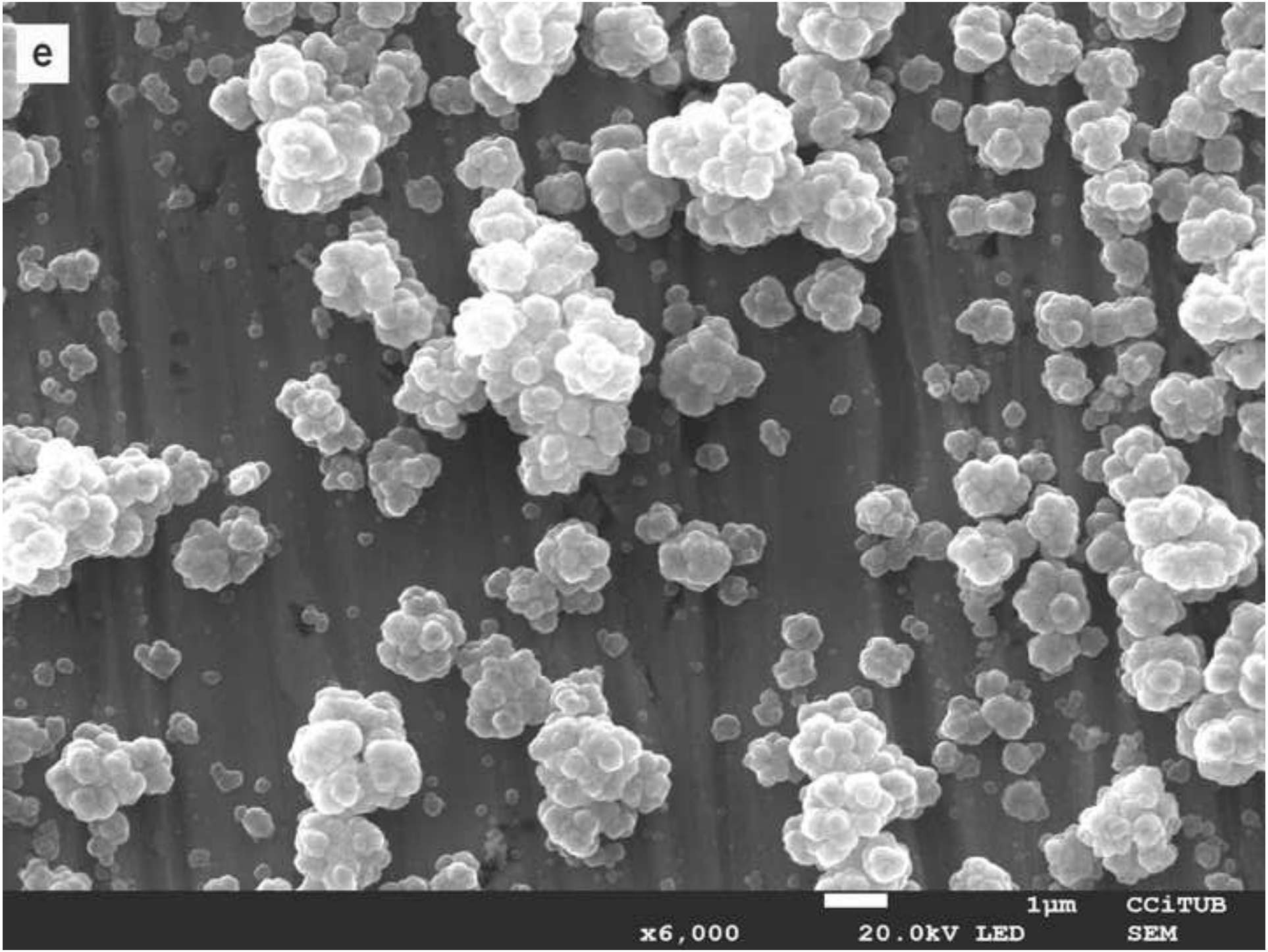

**High-resolution Figure(s)**
**Click here to download high resolution image**

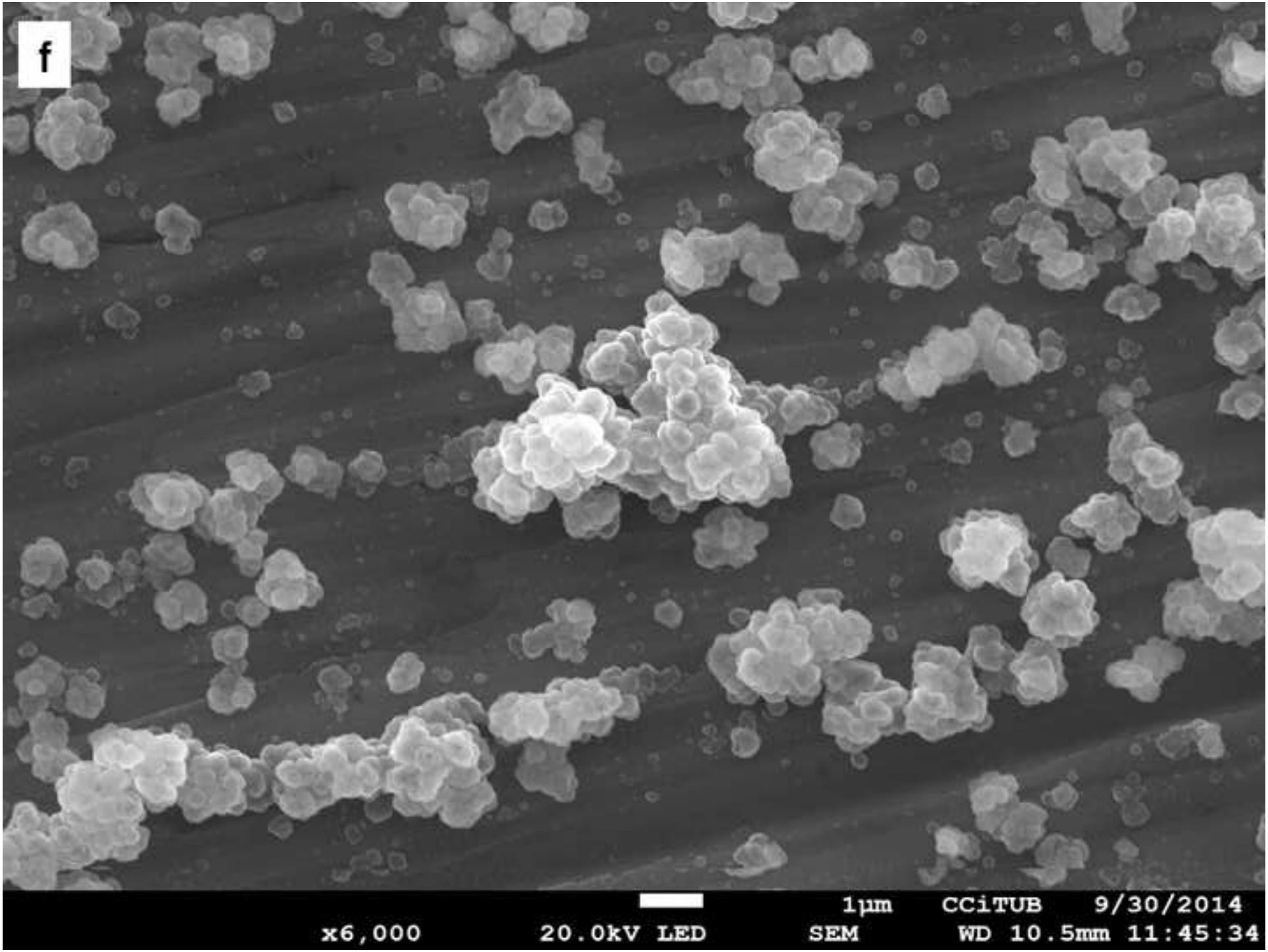

**High-resolution Figure(s)**
**Click here to download high resolution image**

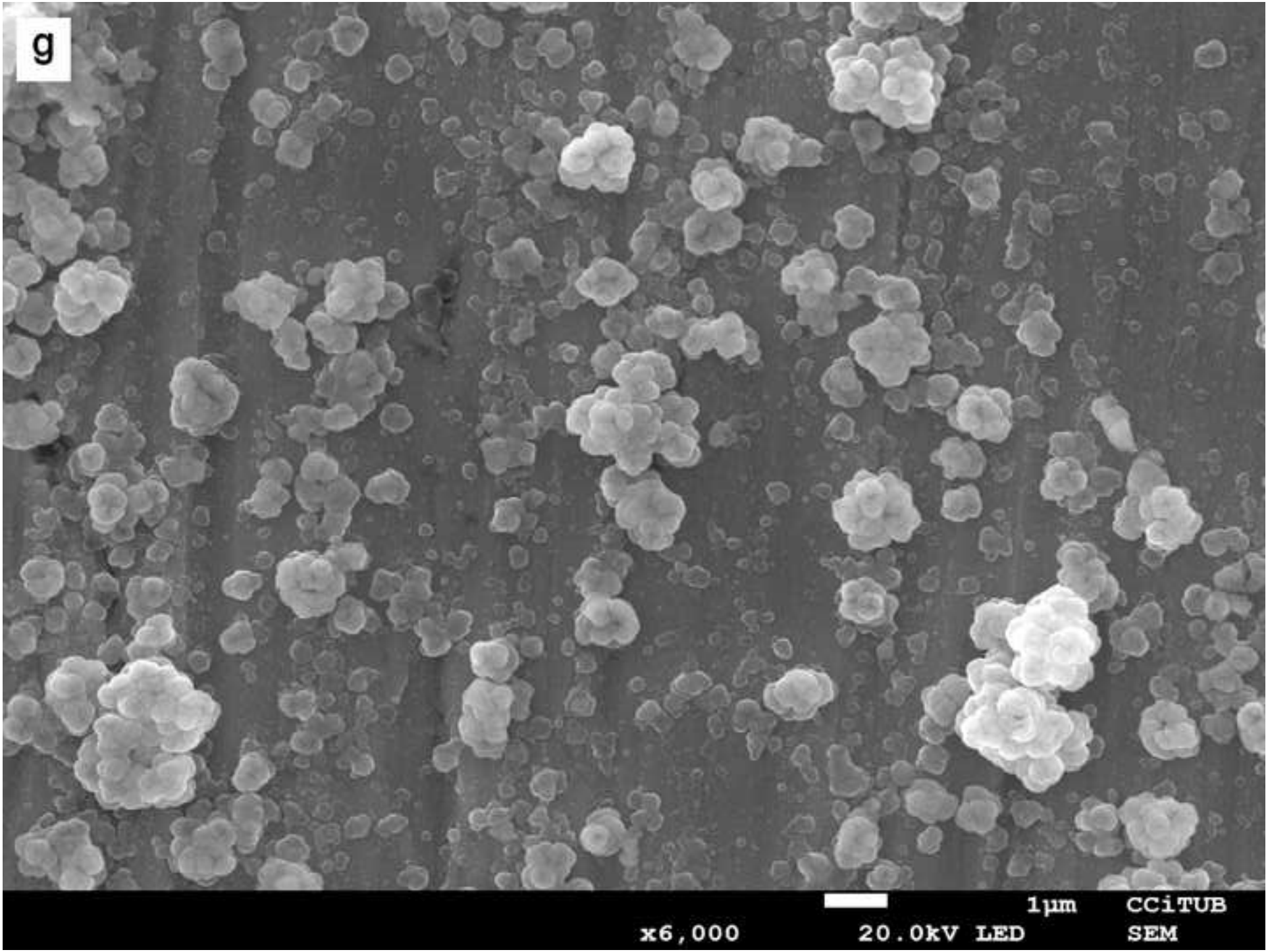

**High-resolution Figure(s)**
**Click here to download high resolution image**

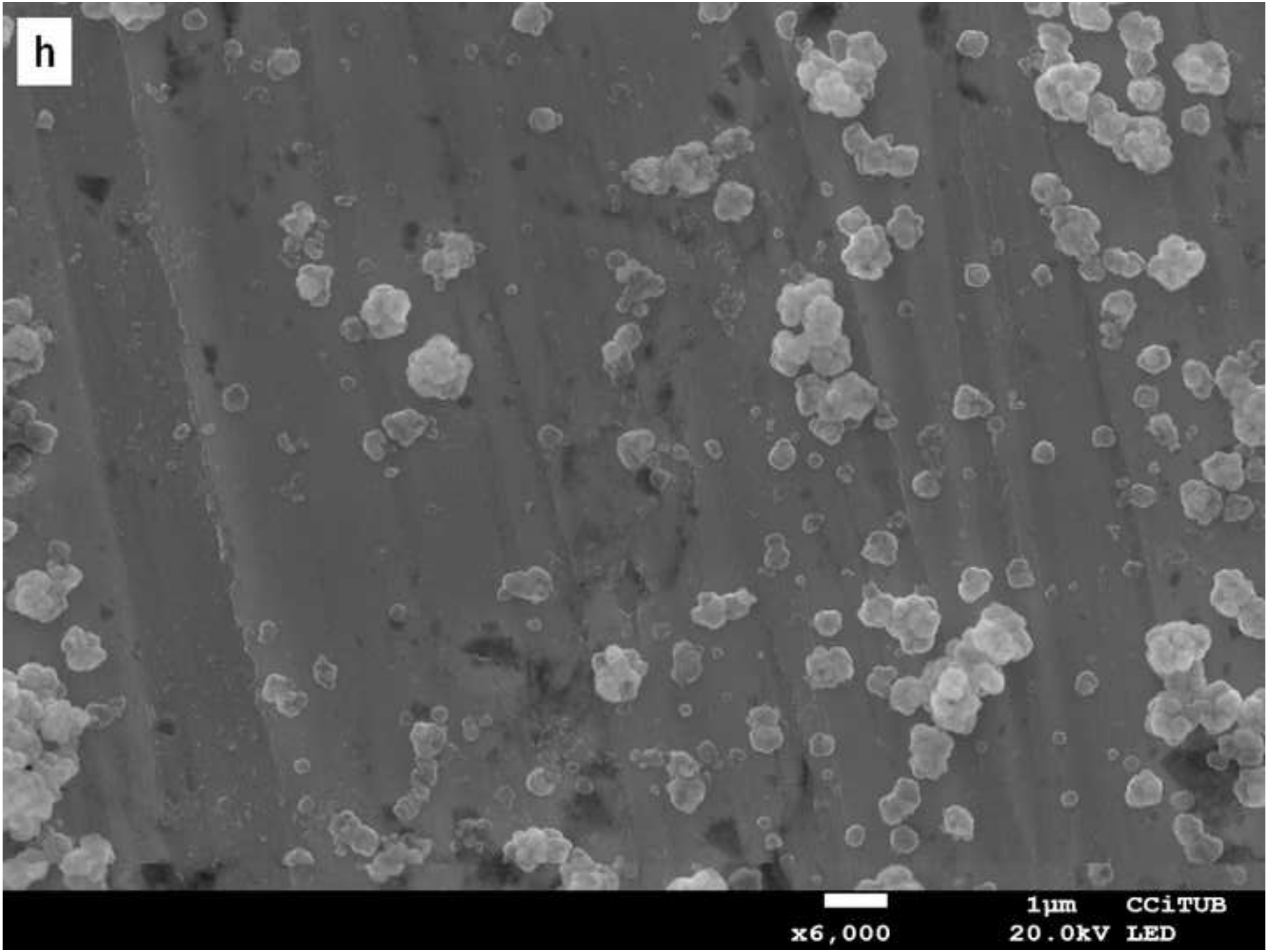

**High-resolution Figure(s)**
**Click here to download high resolution image**

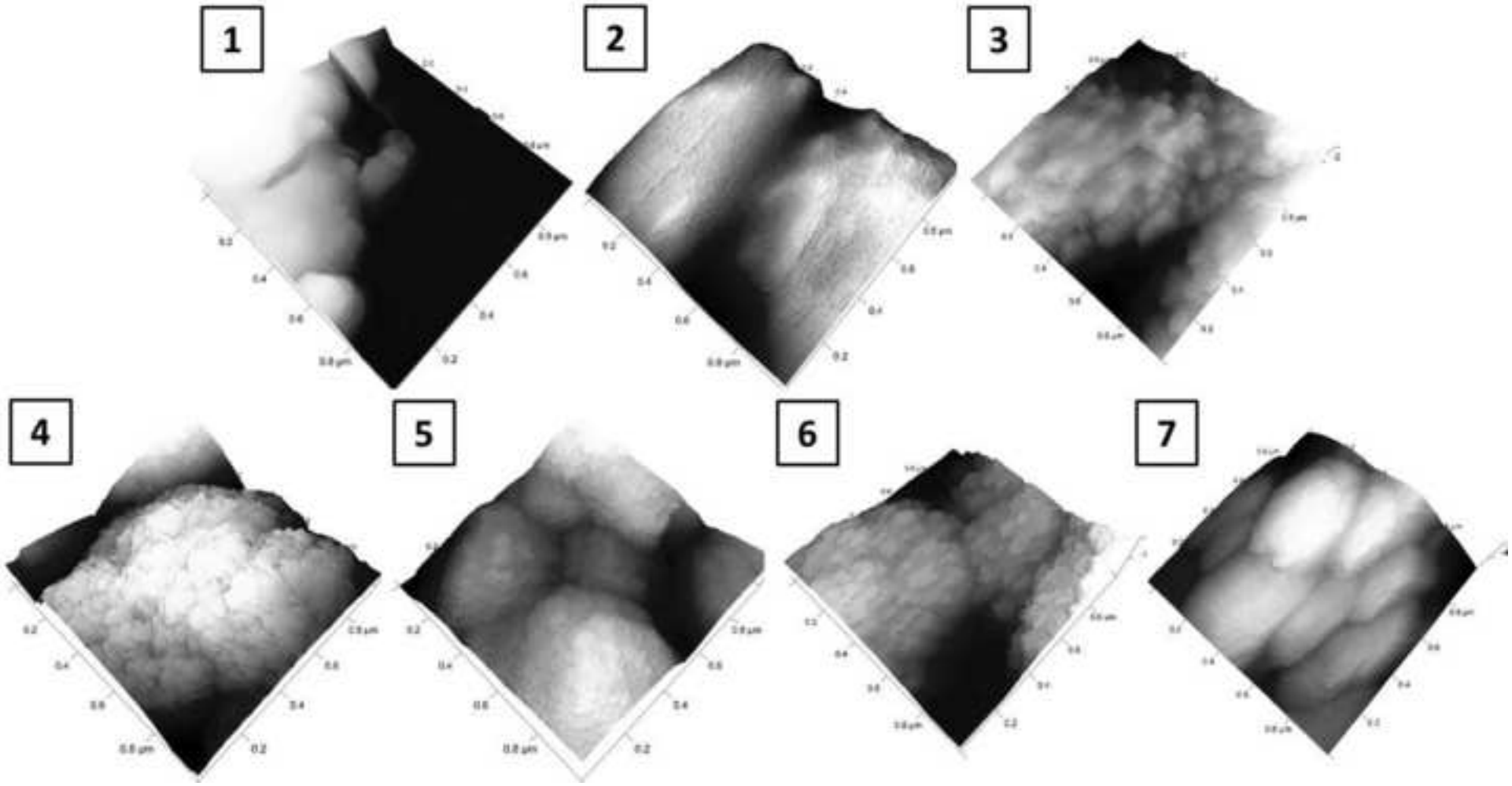

**High-resolution Figure(s)**
**Click here to download high resolution image**

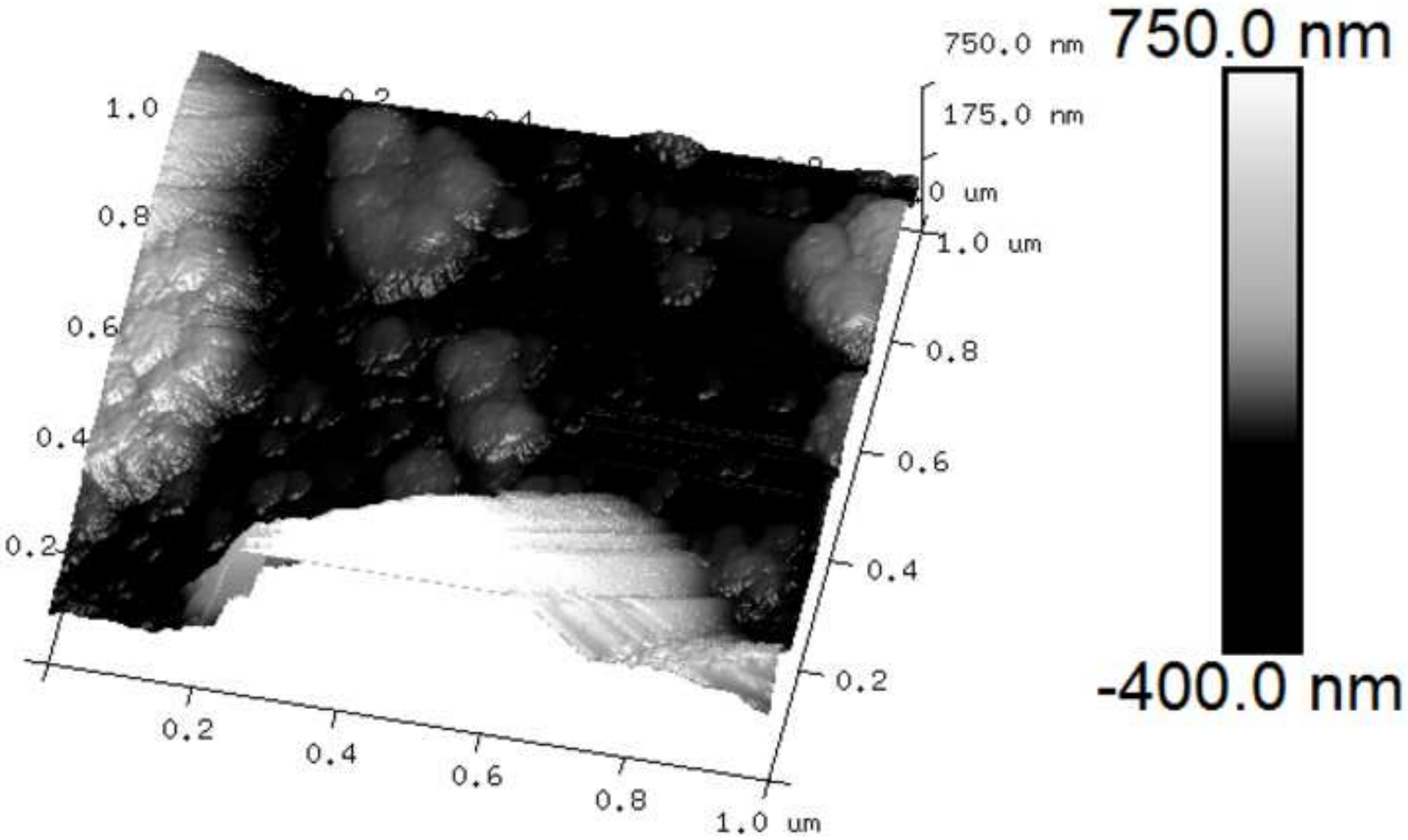

**High-resolution Figure(s)**
**Click here to download high resolution image**

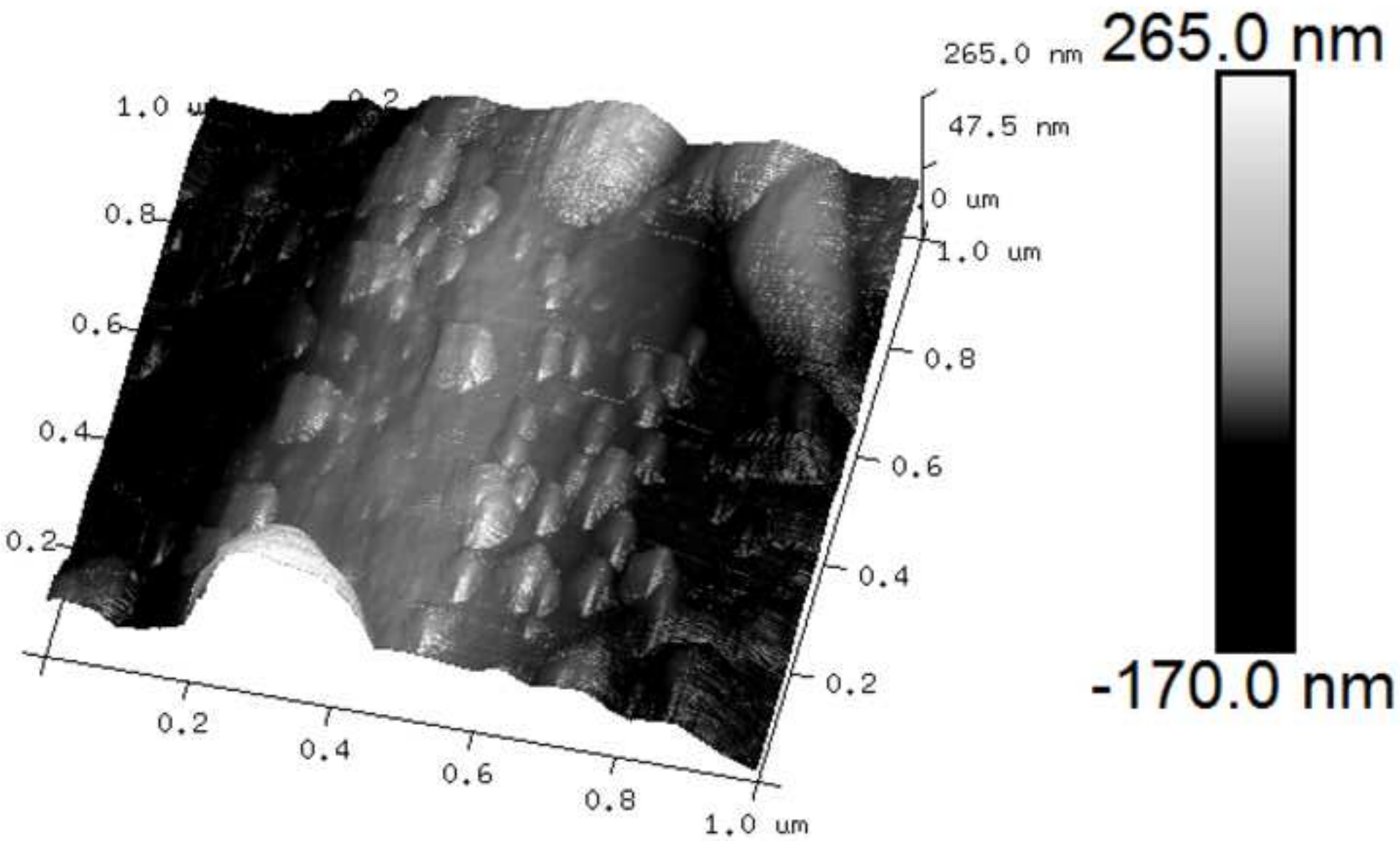

**High-resolution Figure(s)**
**Click here to download high resolution image**

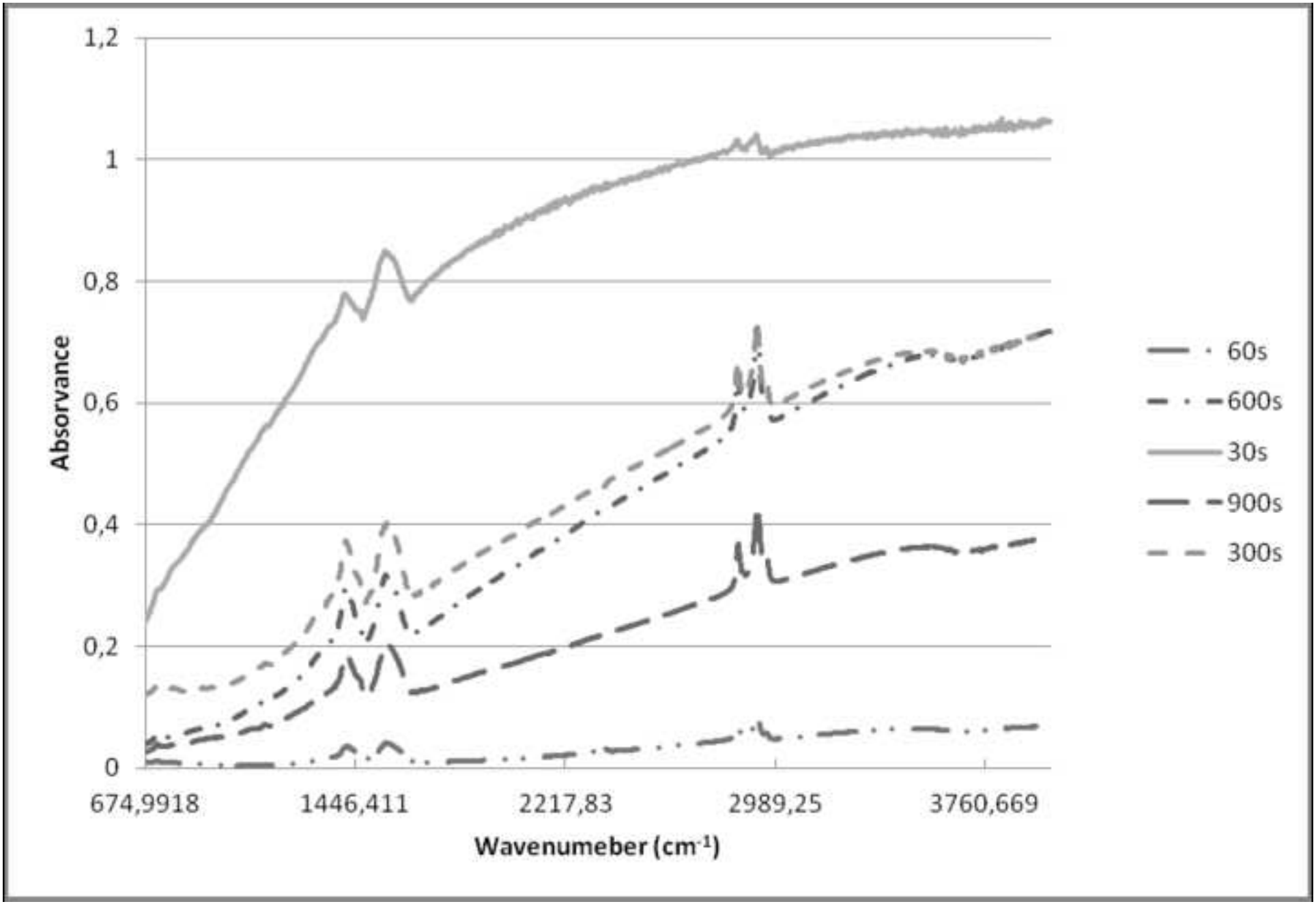

**High-resolution Figure(s)**
**Click here to download high resolution image**

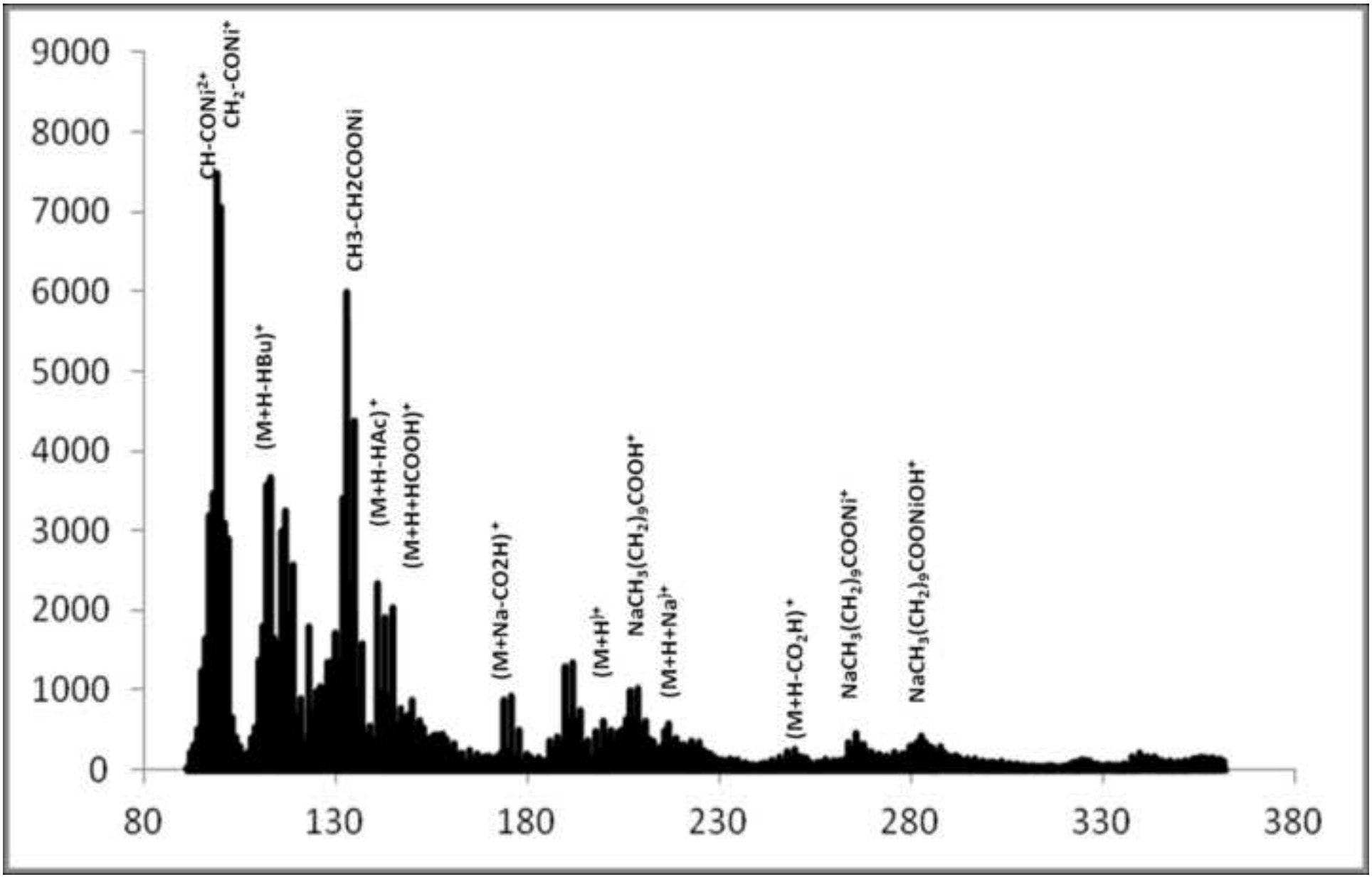

**High-resolution Figure(s)**
**Click here to download high resolution image**

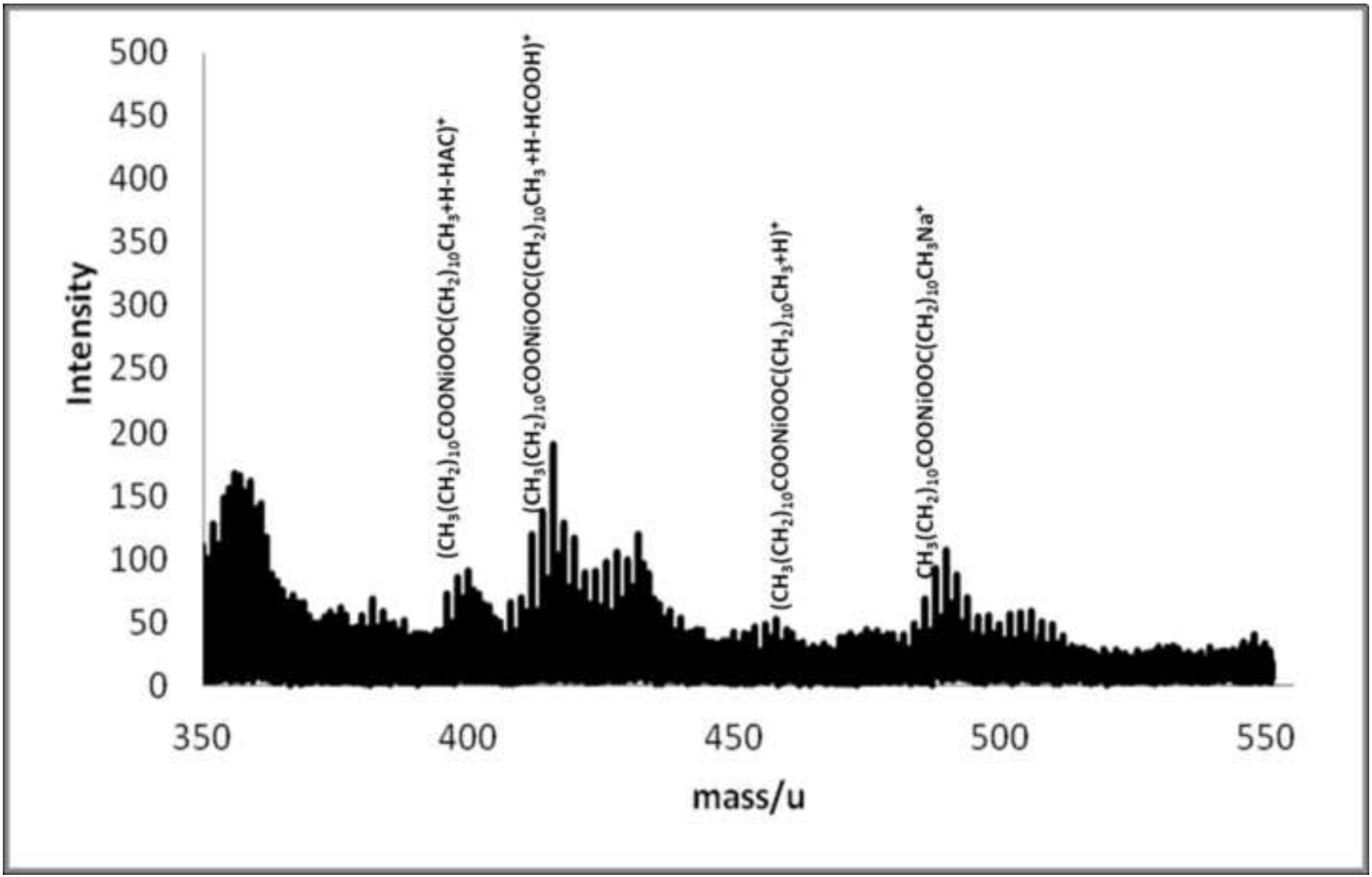

**High-resolution Figure(s)**
**Click here to download high resolution image**

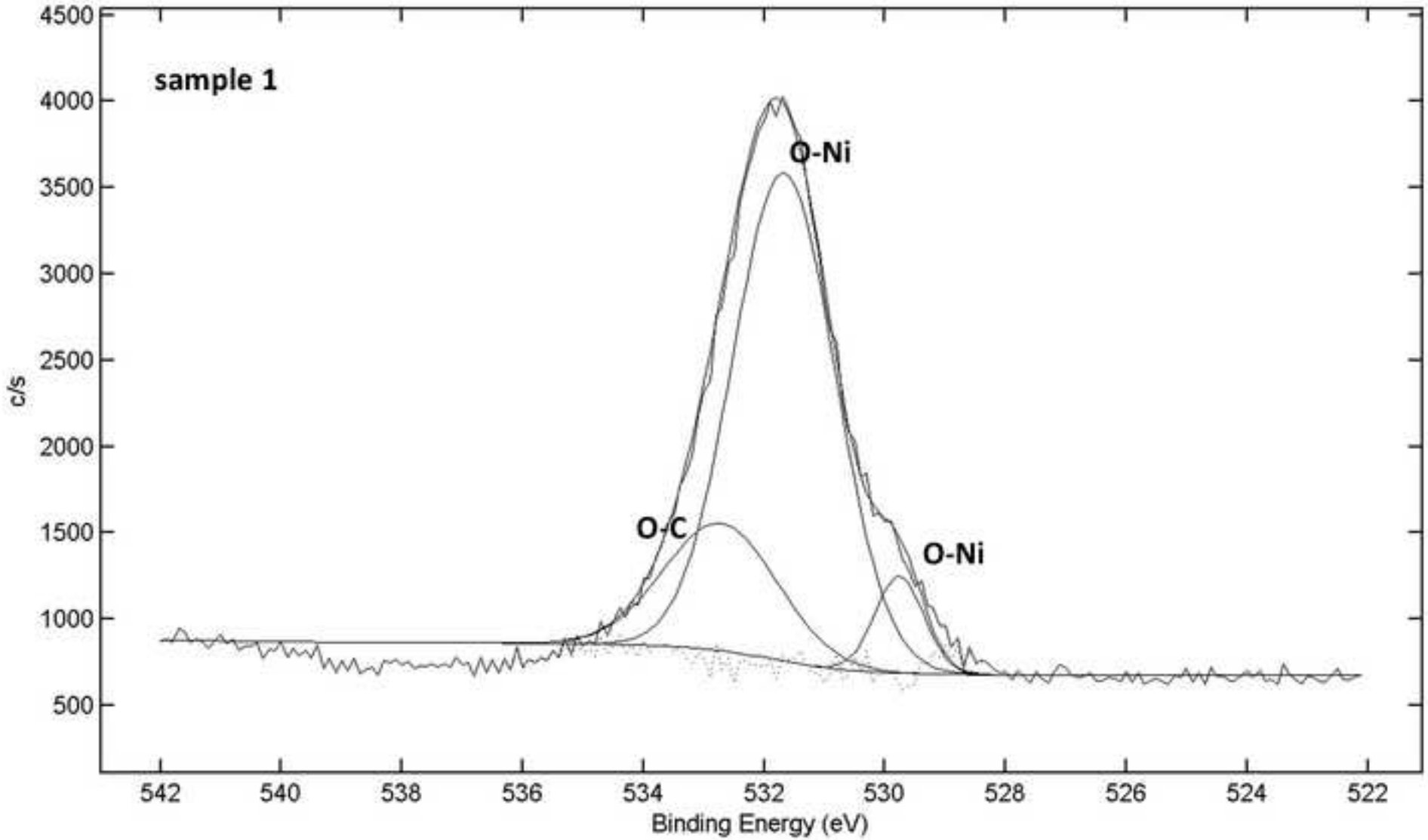

**High-resolution Figure(s)**
**Click here to download high resolution image**

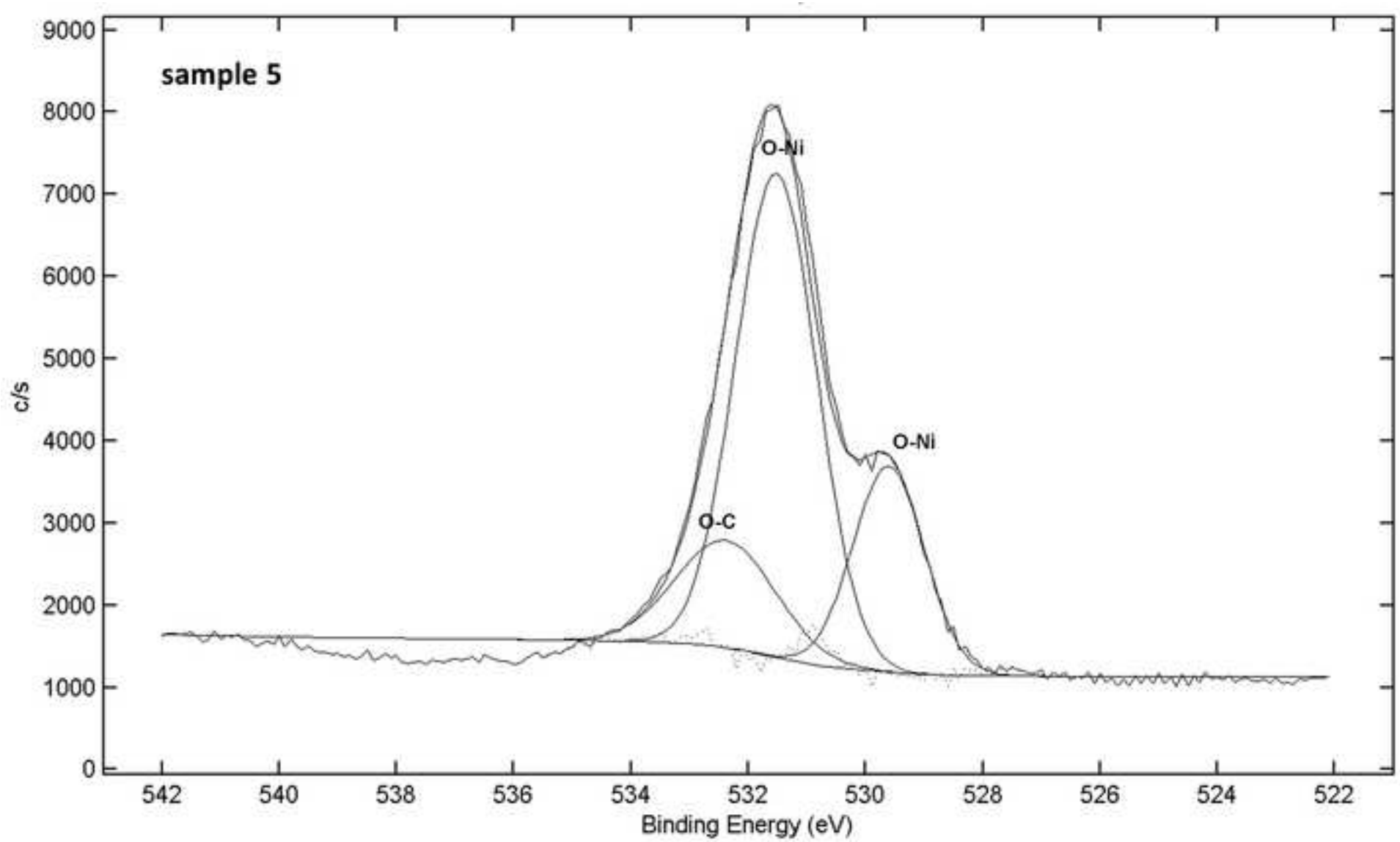

**High-resolution Figure(s)**
**Click here to download high resolution image**

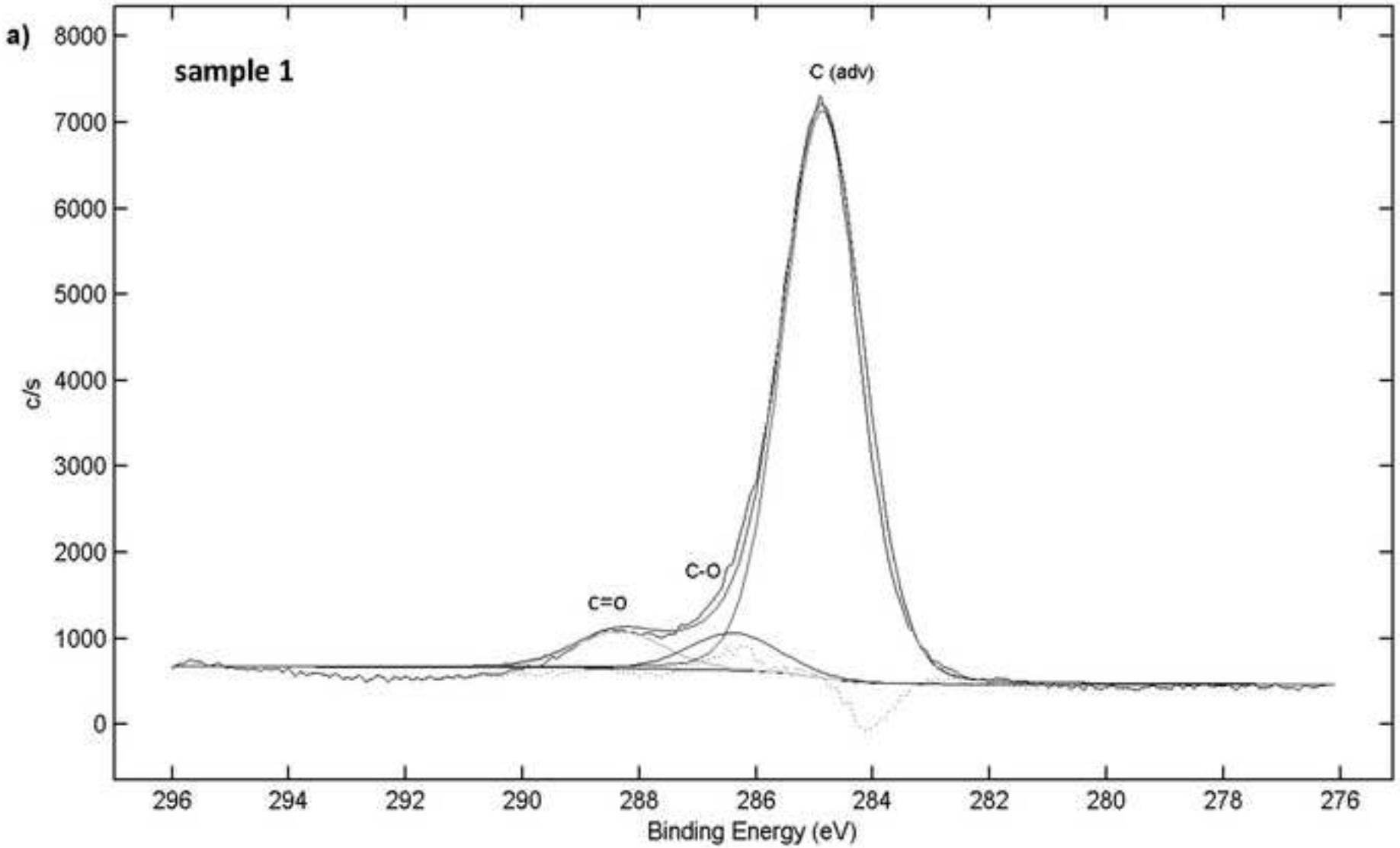

**High-resolution Figure(s)**
**Click here to download high resolution image**

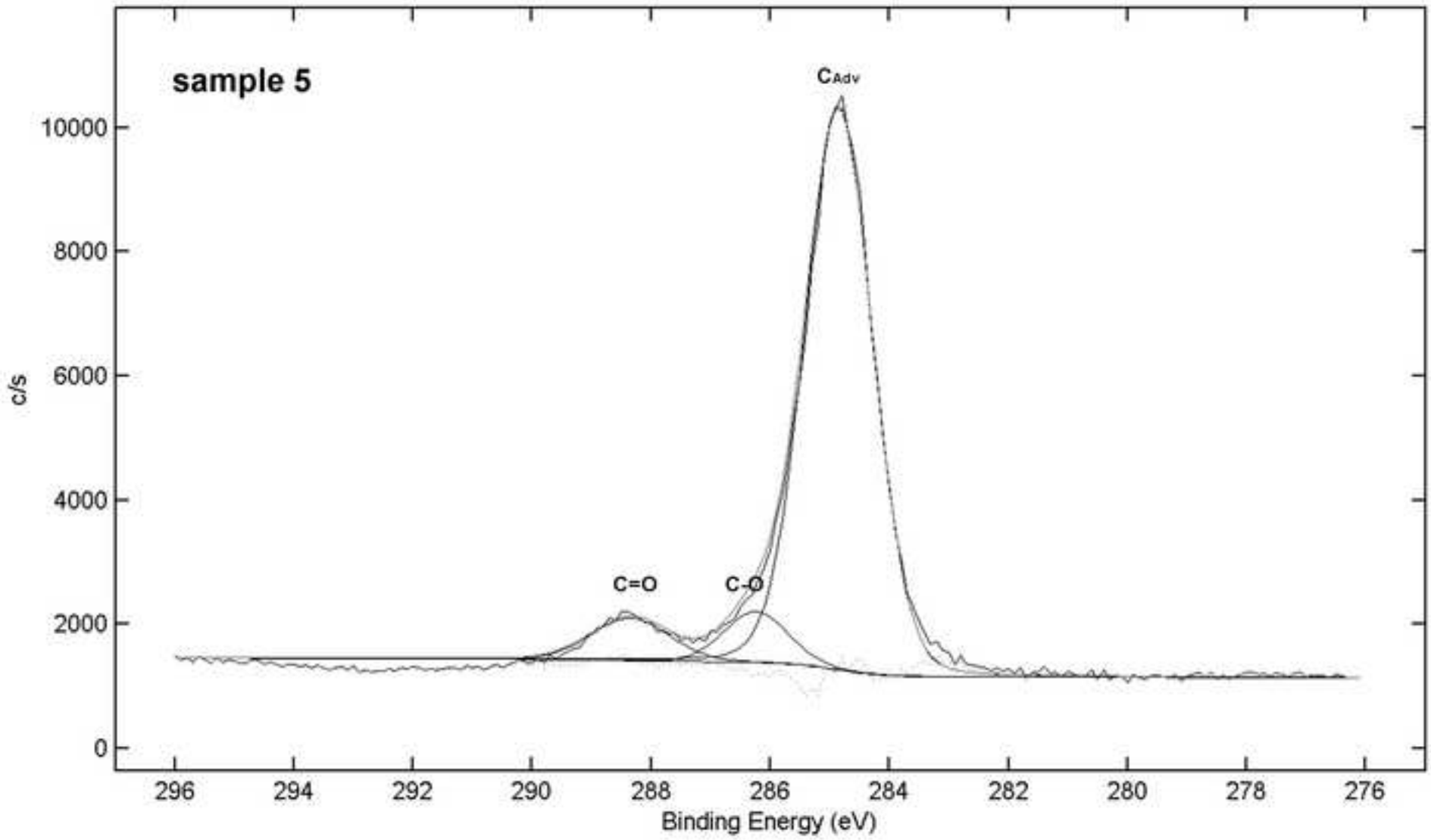

**High-resolution Figure(s)**
**Click here to download high resolution image**